



MICo-150K: A Comprehensive Dataset Advancing Multi-Image Composition

Xinyu Wei^{1,4*}, Kangrui Cen^{4*}, Hongyang Wei^{2,4*}, Zhen Guo^{1,4}, Bairui Li^{1,4},
Zeqing Wang^{3,4}, Jinrui Zhang^{1,4}, Lei Zhang^{1,4†}

¹Hong Kong Polytechnic University ²Tsinghua University ³Sun Yat-Sen University ⁴OPPO Research Institute

Abstract

In controllable image generation, synthesizing coherent and consistent images from multiple reference inputs, i.e., **Multi-Image Composition** (MICo), remains a challenging problem, partly hindered by the lack of high-quality training data. To bridge this gap, we conduct a systematic study of MICo, categorizing it into 7 representative tasks and curate a large-scale collection of high-quality source images and construct diverse MICo prompts. Leveraging powerful proprietary models, we synthesize a rich amount of balanced composite images, followed by human-in-the-loop filtering and refinement, resulting in **MICo-150K**, a comprehensive dataset for MICo with identity consistency. We further build a **Decomposition-and-Recomposition (De&Re)** subset, where 11K real-world complex images are decomposed into components and recomposed, enabling both real and synthetic compositions. To enable comprehensive evaluation, we construct **MICo-Bench** with 100 cases per task and 300 challenging De&Re cases, and further introduce a new metric, **Weighted-Ref-VIEScore**, specifically tailored for MICo evaluation. Finally, we fine-tune multiple models on **MICo-150K** and evaluate them on **MICo-Bench**. The results show that MICo-150K effectively equips models without MICo capability and further enhances those with existing skills. Notably, our baseline model, **Qwen-MICo**, fine-tuned from **Qwen-Image-Edit**, matches **Qwen-Image-2509** in 3-image composition while supporting arbitrary multi-image inputs beyond the latter’s limitation. Our dataset, benchmark, and baseline collectively offer valuable resources for further research on Multi-Image Composition. Project Page: <https://MICo-150K.github.io/>

1. Introduction

With the rapid advancement of generative AI, the capability of image synthesis has expanded dramatically. Both text-to-image (T2I) [7, 11, 22, 24, 25, 28, 29, 32, 36, 39, 50, 55, 59, 70, 83] and image-to-image (I2I) [6, 20, 37, 42, 45, 51, 75, 76, 80, 81, 84, 94] models can produce visually stunning and photorealistic results. Mean-

while, these models have possessed richer world knowledge and can support an increasingly diverse set of condition modalities [48, 56, 95], ranging from complex textual prompts to depth maps, sketches, and reference images. Among them, generating new images following the textual intent of users while maintaining identity (ID) consistency with reference images (particularly facial ID [10, 16, 17, 26, 38, 60, 61, 68, 77, 92]), a task often referred to as personalized generation [53, 54, 78] or in-context generation [37, 65, 85, 97], represents one of the most valuable capabilities of modern generative models. Recent works such as FLUX.Kontext [37] and Qwen-Image [83] have made remarkable progress in this direction. However, these systems only support a single-reference input, limiting the ability to integrate multiple entities into a unified and coherent composition, restricting users’ freedom of creative design.

Multi-Image Composition (MICo) with identity consistency, which involves combining content from multiple source images into a coherent target image while faithfully adhering to the textual prompts, stands as one of the most challenging yet underexplored tasks in generative image modeling. Proprietary models like GPT-Image-1 [63], Nano-Banana [18], and Seedream 4.0 [62] have pushed this task to a new level of realism, coherence, and controllability. However, open-source community remains a significant gap in MICo compared to proprietary models, partly due to the lack of high-quality datasets tailored for this task.

ConceptBed [53] provides a large-scale dataset of ID-preserving images across varying concepts but does not include MICo data. Echo-4o [93] introduces such data only as a small subset, with limited diversity in sources and prompts. Some approaches achieve MICo without explicitly constructing composed targets [14, 54, 91]. Another line of research [47], as shown in Fig. 1, constructs training pairs by segmenting instances from full images using GroundingDINO [44] and SAM [33] as sources while originals as targets [9, 31]. However, such paradigms often yield incomplete and semantically ambiguous samples. Later methods such as UNO [85], OmniGen2 [84], and DreamO [49] enhance semantic richness by synthesizing new contexts; however, the weak generative backbones they used lead to highly homogeneous results in both style and

* Equal contribution. † Corresponding author.

content. Recently, DreamOmni2 [86] introduces a three-stage data generation pipeline, achieving more controllable and consistent compositions. Nevertheless, the synthesized data still suffer from stylistic and contextual homogeneity.

In summary, existing MICO datasets face two main limitations: (1) many source or target images are generated by a few fixed T2I models, leading to homogeneous content and a noticeable quality gap compared to proprietary counterparts; (2) datasets based on real photos or video clips are limited in diversity, lacking imaginative scenarios, and biasing toward person-centric compositions, with insufficient coverage of object-centric or multi-subject cases.

To address these limitations, we introduce **MICO-150K**, a high-quality and comprehensive dataset specifically designed for multi-image composition tasks. We first define a taxonomy with **3 major categories**, **7 sub-tasks**, and **27 fine-grained types**, along with a realistic **Decompose and Recompose (De&Re) track**, as illustrated in Fig. 2. For each task, we design dedicated data collection and cleaning pipelines to curate high-quality source images of objects, humans, clothing, and scenes. Each image is paired with a detailed, descriptive caption aligned with its visual content. To generate composition prompts, we use GPT-4o [51] with a **Compose-by-Retrieval** strategy, which combines compatible source captions to form rich and coherent prompts for each composition type. These prompts are then fed into Nano-Banana [18], a state-of-the-art proprietary model, to synthesize high-quality composite images. Finally, a human-in-the-loop post-filtering process is applied to retain only the most accurate and visually consistent results, yielding the final MICO-150K dataset.

It is also observed that there lacks a dedicated benchmark for evaluating MICO performance. To fill this gap, we introduce **MICO-Bench**, a comprehensive benchmark comprising 1,000 carefully curated cases, 100 for each of the seven MICO sub-tasks and 300 challenging cases in the De&Re subset. Each case is rigorously validated by human annotators to ensure diverse semantics and scene coverage across source images and text prompts. For evaluation, we propose a new metric **Weighted-Ref-VIEScore**, a reliable and human-aligned metric for assessing MICO performance.

We fine-tune several T2I models, BAGEL [19], BLIP3-o [12], Lumina-DiMOO [89], OmniGen2 [84], and Qwen-Image-Edit [83] on **MICO-150K** and evaluate them using **MICO-Bench**. BLIP3-o and Lumina-DiMOO that originally lacked multi-image composition capabilities acquire strong MICO abilities after fine-tuning. BAGEL and Qwen-Image-Edit, though not explicitly trained for multi-image composition, demonstrate emergent MICO capability that is significantly enhanced after fine-tuning on MICO-150K. OmniGen2, which already possesses robust multi-image consistency, also exhibits further improvement after training. Among these, the model fine-tuned from Qwen-Image-



Figure 1. Previous MICO methods typically collect high-quality images or video frames as **target images** (1). Using Open-Vocabulary Detectors (OVD) [44] and SAM [33], objects within targets are segmented to obtain **source images** (2). Some methods enhance the targets by retrieving additional frames of the same subject from videos (3), or enhance the sources using S2I (Subject-to-Image) or inpainting models (4). Training pairs are then constructed along multiple paths: (2→1), (2→3), (4→1), and (4→3). However, the masks in (2) are often incomplete and semantically ambiguous; the generated images in (4) tend to share similar styles, content, and limited diversity due to reliance on a few fixed generative models; the frames in (3) originate from a small number of high-quality videos, leading to limited scene variety and a lack of imaginative or complex multi-subject scenarios.

Edit, termed **Qwen-MICO**, serves as our primary baseline. In summary, our contributions are threefold: (i) We introduce **MICO-150K**, a large-scale high-quality dataset specifically designed for multi-image composition with identity consistency, and provide comparisons between real-world and synthetic compositions.; (ii) We present **MICO-Bench** along with the **Weighted-Ref-VIEScore**, establishing a comprehensive and reliable evaluation framework for MICO task; (iii) We observe that some strongly pretrained I2I models **naturally exhibit emergent MICO capabilities**.

Extensive experiments further demonstrate the robustness and generality of MICo-150K, as models with diverse architectures and initialization states consistently achieve substantial improvements after fine-tuning. (iv) We propose **Qwen-MICo** as a baseline. Trained solely on MICo-150K, it outperforms Qwen-Image-2509 [57] in 3-image composition while lifting the restriction to support (> 3) references.

2. Related Work

Training-free MICo Methods. Versatile Diffusion [91], trained solely on standard I2I data, adopts a unified multi-flow diffusion framework optimized across diverse tasks, exhibiting certain MICo capabilities. λ -ECLIPSE [54] learns the CLIP latent space using image-text interleaved data and achieves MICo through a frozen diffusion inference backend without any specific supervision. MIP-Adapter [31] introduces lightweight, learnable adapters into a frozen diffusion model, enabling MICo by training a small adapter. LAMIC [14] extends single-reference T2I models in a fully training-free manner by introducing *Group Isolation Attention* and *Region-Modulated Attention*, which support layout-aware MICo without modifying the underlying MMDiT parameters or requiring additional training data.

Trainable MICo Methods. Subject Diffusion [47] pioneers a data construction paradigm that extracts background-free instances using GroundingDINO [44] and SAM [33] as source images, with the original images serving as targets. This strategy has provided valuable insights for building MICo datasets. MS-Diffusion [78] follows this approach but constructs semantically aligned image pairs from different frames of the same object in video clips, avoiding direct copy-paste duplication. UNO [85] enhances model capability through progressive cross-modal alignment. It follows Subject Diffusion [47] but employs a Subject-to-Image (S2I) model to generate new source images rather than using the original instances directly. DreamO [49] introduces *feature routing constraints* into the DiT training process to ensure identity consistency. It uses PuLID [26] to generate multiple portraits of the same person ID and selects different frames of the same subject from videos for body-level data. OmniGen2 [84] employs two distinct decoding pathways for text and image with unshared parameters and achieves strong MICo ability through large-scale training. Its data pipeline also leverages multi-frame videos but includes refined filtering and inpainting strategies to restore background context. XVerse [9] introduces a *T-Mod Resampler* that processes each source image and injects its representation into a per-token modulation adapter, while incorporating VAE features to preserve fine-grained details. DreamOmni2 [86] proposes a novel three-stage data construction pipeline. It first introduces *dual-branch attention mixing* in a T2I model to generate two semantically aligned images with partially

shared features, then trains an extraction model on them, which is subsequently used to generate reference images.

3. MICo-150K Dataset

This section provides the detailed construction pipeline of the **MICo-150K**. Sec. 3.1 describes the collection of source images, while Sec. 3.2 details the construction processes of the four task categories. For clarity, the number of cases for each sub-task is summarized in Tab. 1, representative examples from each task are illustrated in Fig. 3. All image licensing and usage permissions are detailed in Sec. 7.1.

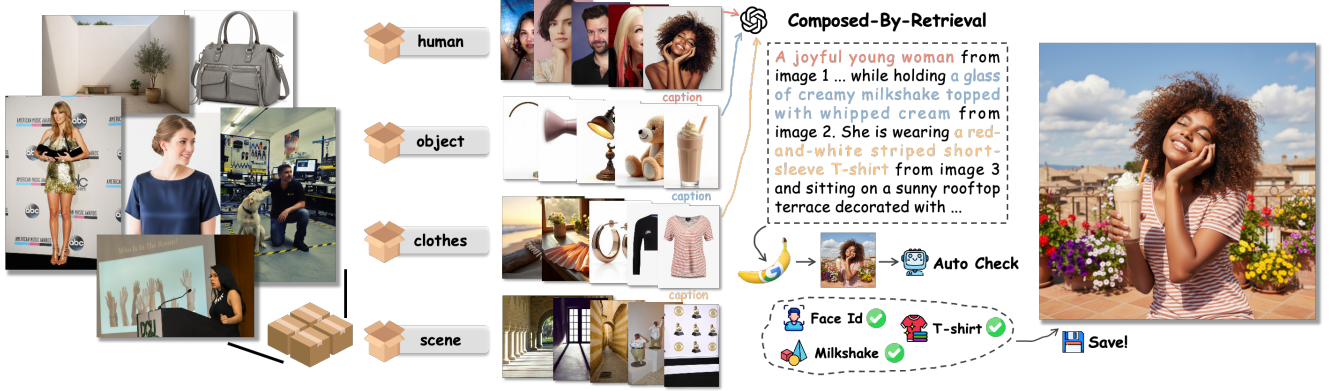
3.1. Source Image Collection

Object Images. We collected object images and the corresponding captions from the Subject200k [66] dataset. To ensure quality, we employed **Qwen2.5-VL-72B** [3] for filtering, removing images containing humans, obvious blur, corruption artifacts, or ambiguous semantics. Each retained image was assigned a detailed, descriptive caption and category label. Within each category, we extracted visual features using **DINO-v3** [64] and **SigLIP2** [71], concatenated them, and applied **DBSCAN** [23] clustering to eliminate redundancy, keeping only one representative image per visual-semantical cluster. After this rigorous cleaning process, we obtained **31.5K** high-quality object images.

Human Images. We collected 13.7K high-quality model images from the VITON-HD [15] try-on dataset, 6K upper-body portraits from the Headshot iStockPhoto dataset [4], 3K high-resolution portraits from the Headshot Pexels v1 dataset [5], professional portrait photos from the X2I-Subject-Driven dataset [88], and 144K photos of 5,403 celebrities. We then employed **Qwen2.5-VL-72B** [3] to remove images containing multiple faces, back views, or heavily occluded faces. Each remaining image was annotated with a detailed caption describing gender, attributes, clothing, and posture. After the cleaning and annotation process, we obtained **44.6K** high-quality human portraits, ensuring maximal diversity in facial identities. A detailed analysis of human-face images is provided in Sec. 7.3.

Cloth Image. We collected clothing images from the Subject200k [66] and the VITON-HD [15] try-on dataset. The clothing items were categorized by type (upper garments, lower garments, shoes, accessories) and gender, forming $4_{type} * 2_{gender} = 8$ subcategories in total. We used **Qwen2.5-VL-72B** [3] to filter out unclear or inappropriate items and generate descriptive captions for each image. The final source pool contains **17.3K** upper garments, **1.3K** pants, **428** pairs of shoes, and **7.8K** accessories.

Scene Images. We collected scene images from the Mulan [72], Echo-4o [93], and SUN397 [87] datasets. However, the overall quality of these scenes varies significantly.



(a) High-quality open-source data are collected and cleaned through a dedicated pipeline, categorized into four groups: **human**, **object**, **clothes**, and **scene**, each with detailed captions. For each task, a diverse set of source images is randomly sampled from these categories, and a multi-image composition prompt is generated by GPT-4o using image captions under a “**Composed-by-Retrieval**” strategy. The generated prompt is then fed into Nano-Banana [18] to synthesize composite images. Each output image undergoes an automated verification process including QwenVL2.5-72B [3] and ArcFace [21] to ensure that all source images are correctly represented in the final composition before being included in the dataset.



(b) We collect a large number of high-quality single-person portraits through our data-cleaning pipeline and use Nano-Banana [18] to **decompose** each image into its constituent components—**scene**, **human**, **objects**, and **clothes**. Human annotators then carefully inspect all decomposed components to ensure their quality. Once all parts meet the required standards, Nano-Banana is used again to **recompose** them into a complete image.

Figure 2. Construction pipeline of MICO-150K. (a) The data construction pipeline for the **Human-Centric**, **Object-Centric**, and **HOI (Human-Object Interaction)** tasks. (b) The pipeline for the **De&Re (Decompose and Recompose)** task.

Table 1. Statistics of the **MICO-150k** dataset. The dataset is carefully balanced to ensure diversity across task types and input images. In the **Types** column, abbreviations denote component categories: O = Object, S = Scene, P = Person, M = Man, W = Woman, and C = Cloth.

Task	Sub-task	Types	Count
Object Centric	Object + Scene	1O1S, 2O1S	5014, 4999
	Object + Object	2O, 3O, 4O, 5O	10007, 10012, 5001, 4998
Person Centric	Person + Person	1M1W, 2M1W, 2W1M 2M, 2W, 3M, 3W	3001, 3003, 3066 2996, 3006, 2999, 2991
	Person + Scene	1P1S, 2P1S	4986, 4994
	Person + Objects	1P1O, 1P2O, 2P1O, 2P2O	5020, 4973, 5071, 5050
Human Object Interaction	Person + Clothes	1P1C, 1P2C, 1P3C, 1P4C	7031, 7017, 6942, 6973
	Person + Objects + Clothes	1P1C1O, 1P1C2O	5034, 5022
		1P2C1O, 1P2C2O	5025, 5011
De&Re	Adaptive		11677

To make them suitable, we first filtered out images whose shorter side was below 512 pixels. For the remaining images, we used Qwen2.5-VL-72B [3] to perform a series of quality checks: (1) the scene must be open and contain no people; (2) it should depict a realistic, natural environment

with no visible artifacts; (3) it should be clean and well-organized, without elements such as toilets or garbage; (4) it must not be overly confined and should be spacious enough to accommodate at least one person. In addition, we used GPT-4o [67] to generate extra portrait-friendly scenes. We

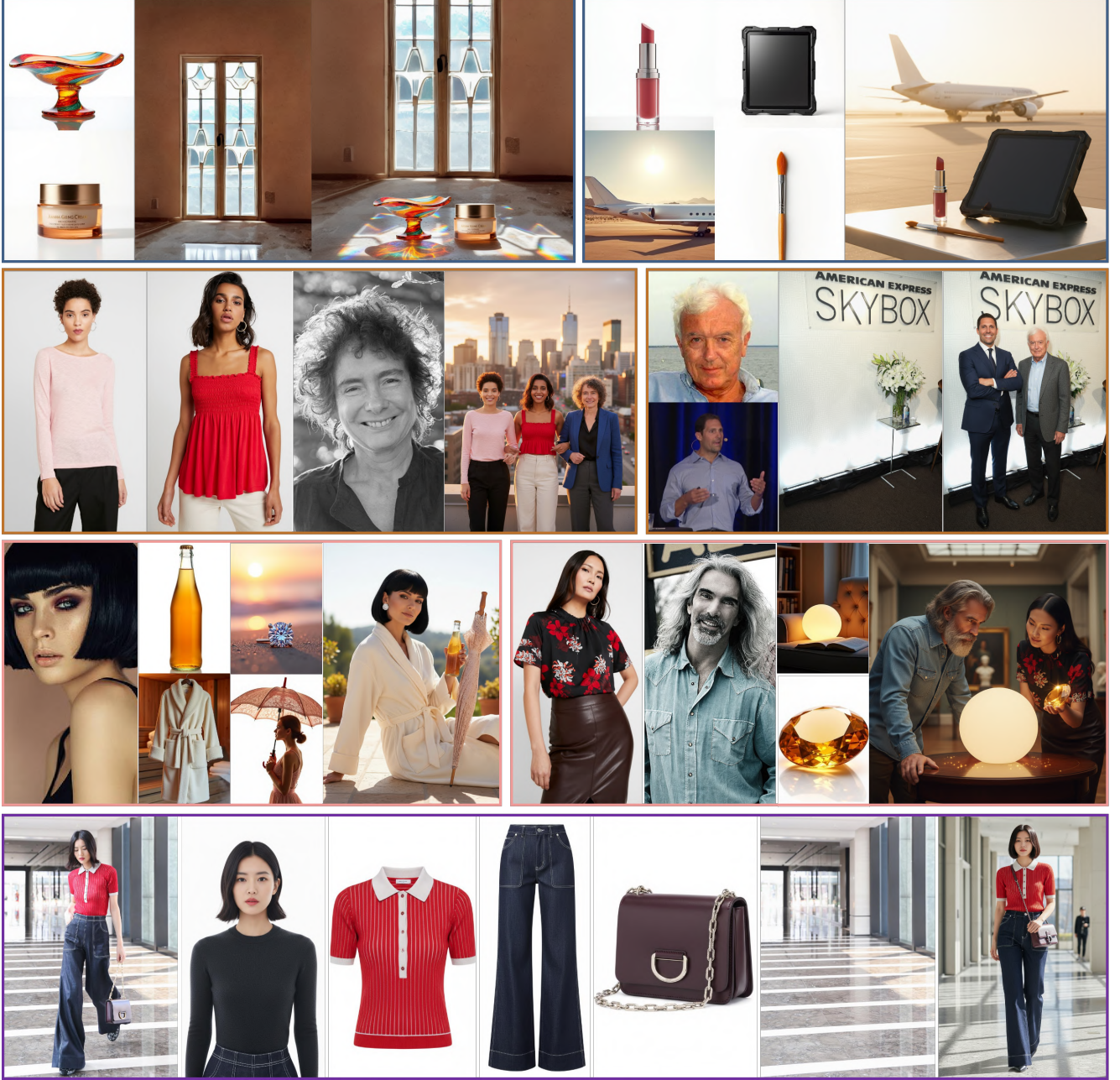
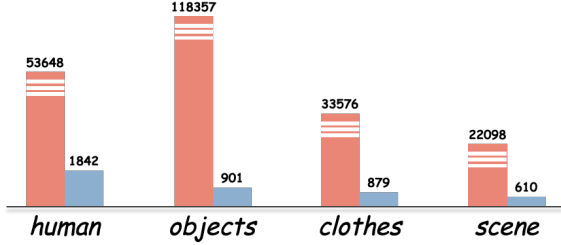


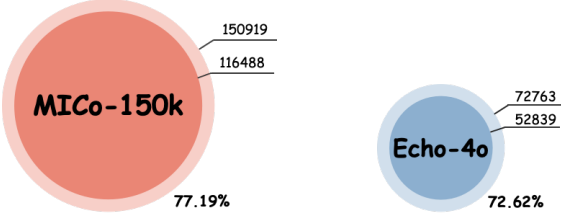
Figure 3. Visualization examples from the MICo-150K dataset. **Row 1 (Object-Centric)**: “2 objects + scene” and “4 objects” compositions. **Row 2 (Person-Centric)**: “3 women” and “2 persons + scene”. **Row 3 (Human-Object Interaction)**: “1 person + 4 objects” and “2 persons + 2 objects”. **Row 4 (De&Re)**: the first image is a real-world photo, the last is the recomposed result, with intermediate visual elements including decomposed persons, objects, clothes, and scene components.

manually collected 200 high-frequency scene descriptions from AIGC community forums used for portrait generation, assigned concise text labels to them, and then prompted GPT-4o to synthesize the corresponding scenes. After all filtering and generation, we obtained a final set of **11K** high-quality scenes suitable for the MICo tasks.

Compose-by-Retrieval. We employ Nano-Banana [18] to compose the source images according to task settings, producing high-quality composite results. However, directly sampling source images at random from the pools may lead to semantically incompatible combinations, for instance, pairing a male athlete with high-heeled shoes, resulting in



(a) Statistics of source image counts across different categories.



(b) Semantic redundancy in text prompts. We extract text embeddings using CLIP and set a cosine similarity threshold of 0.85 to identify duplicates.

Figure 4. High-quality multi-image composition datasets that are non-segmentation-based and not generated by Flux series [37] are extremely rare; to the best of our knowledge, only Echo-4o [93] is publicly available. MICo-150K significantly surpasses it in both source image diversity and text prompt semantic variety.

poor generation quality. To address this, we propose the **Compose-by-Retrieval** strategy. After choosing a primary (subject) image, we sample multiple candidates for clothing, scenes, or objects from respective pools. We then provide the subject image, candidate images, and their detailed captions as the context to GPT-4o [67] to select the most semantically compatible combination for composition.

3.2. Construction of MICo Tasks

Object-Centric Tasks. We define two sub-tasks for object-centric composition. The *Object + Object* task involves combinations of one to four distinct objects, where source images are randomly sampled for composition. The *Object + Scene* task covers compositions of a single object or two objects placed within a specific scene. We adopt the proposed *Compose-by-Retrieval* strategy, which provides multiple candidate scenes for each object and adaptively selects the most semantically compatible one. Previous MICO methods typically use source image captions directly as prompts, such as “Combine 2 images according to <Caption A> and <Caption B>.” To promote prompt diversity and naturalness, we instead treat source captions as contextual input for GPT-4o, which generates a more coherent composition prompt. Furthermore, GPT-4o annotates the prompt with explicit token-to-source mappings, providing a foundation for future studies on latent space alignment. We then used Nano-Banana to synthesize composite images and employed Qwen2.5-VL-72B for verification. Each source image is paired with the generated target, and the model checks whether the objects from

the source appear correctly in the final composition.

Person-Centric Tasks. We define two sub-tasks: *Person + Person*, which covers 7 different gender and group combinations, and *Person + Scene*, which composes 1 or 2 individuals placed within specific scenes. We find that omitting explicit gender specification in prompts degrades generation quality. Therefore, we explicitly state gender information in the *Person + Person* task. For the *Person + Scene* task, we adopt the *Compose-by-Retrieval* strategy to select semantically compatible scenes for each person. During quality control, objects and scenes are verified using Qwen2.5-VL-72B, while face ID consistency is evaluated via ArcFace [21] embeddings. Specifically, we extract face ID embeddings from both the source and generated images and compute the optimal matching using the Hungarian algorithm [35]. A generation is considered valid only if all matched pairs exceed a task-specific similarity threshold.

Human Object Interaction Tasks. We define three sub-tasks: *Person + Object*, *Person + Clothes*, and *Person + Object + Clothes*, each further divided into four task variants as summarized in Tab. 1 (third row). During the composition phase, we explicitly specify the gender of the human source and apply the *Compose-by-Retrieval* Strategy to select semantically compatible objects or clothes for each case. For quality verification, we employ both Qwen2.5-VL-72B and ArcFace. The former ensures that all visual entities are correctly rendered, while the latter extracts face ID and evaluates the consistency with the source images.

Decompose-and-Recompose (De&Re) Tasks. This task is the most complex and comprehensive part in MICo-150K. We first curated a large collection of high-quality single-person portraits from the CC12M [8] dataset. Using Nano-Banana, we decomposed these complex, realistic photographs into separate components such as humans, clothing, objects, and scenes. Human annotators then conducted fine-grained quality checks, identifying failure cases, such as those missing object identities, or directly copy-pasted, lacking sufficient variance. Then, the annotators rewrote component-specific prompts to correctly extract the intended elements. After this human-in-the-loop refinement process, Nano-Banana was used again to recombine them into complete images. Thus, each set of components produces two versions: a real-world composition and a recomposed synthesized one, as illustrated in Fig. 2.

After the above construction process, the statistics of the dataset’s source images and text prompts are shown in Fig. 4, demonstrating significantly greater diversity compared to other datasets [93] with similar functionality.

4. MICo-Bench

We first analyze why conventional image generation metrics are insufficient for MICO task (Sec. 4.1), then introduce the

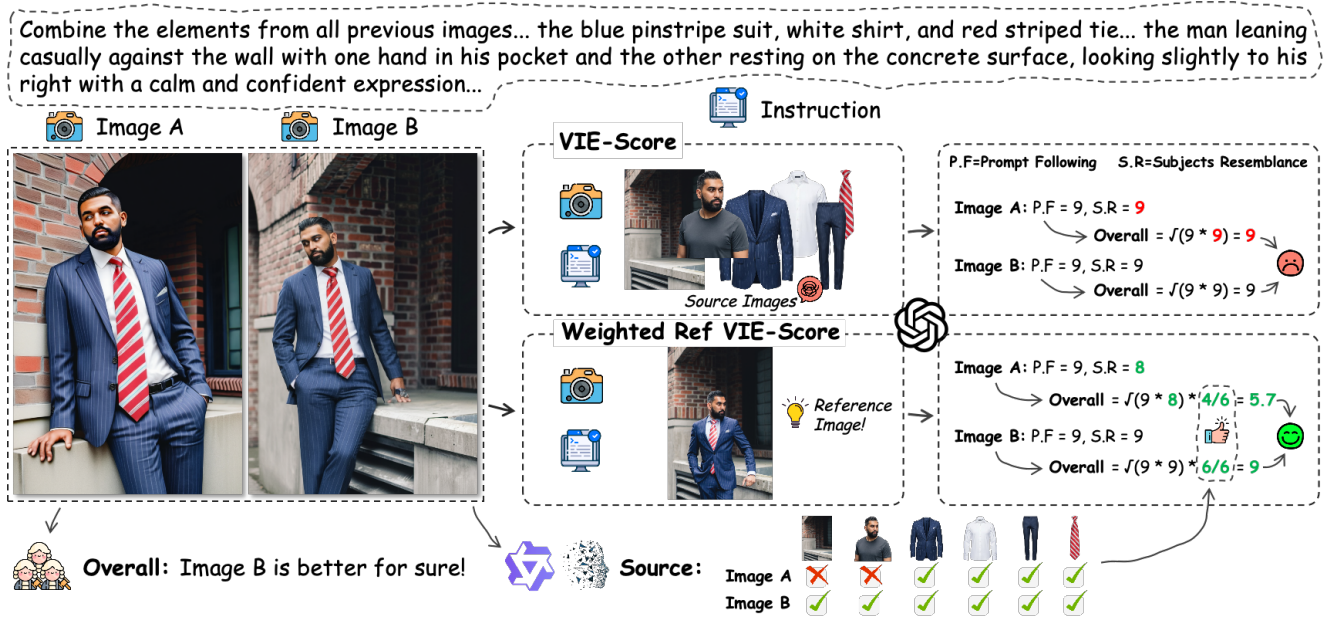


Figure 5. Traditional VIEScore requires inputting all source and generated images into the evaluator, which often leads to degraded performance as **GPT-4o’s cross-image attention becomes overloaded**. This prevents the model from fully understanding each image and accurately determining whether every source appears in the target, resulting in substantial scoring errors (in this example, all the three human evaluators unanimously agreed that Image B was far superior). In contrast, MICO-Bench first assess whether each source image appears in the generated result to produce weights. Each case also includes a verified reference image that contains all sources. During evaluation, GPT-4o compares only the generated image and the reference image, enabling human-level judgment accuracy.

Weighted-Ref-VIEScore (Sec. 4.2). Finally, we describe the curation pipeline of our benchmark (Sec. 4.3).

4.1. Why Existing I2I Metrics Fail for MICO?

With the rapid rise of general-purpose Vision-Language Models (VLMs), evaluating generative tasks such as I2I and T2I through VLMs has become increasingly popular. VIEScore [34] offers a representative framework for VLM-based image evaluation by decomposing overall quality into two dimensions: Semantic Consistency (SC) and Perceptual Quality (PQ). The final score is computed as $SC \times PQ$. OmniContext Bench [84] follows this framework and employs GPT-4o [67] to evaluate the SC score of composition results in terms of Prompt Following (PF) and Subject Resemblance (SR). However, it has a key limitation: it requires all source images to be input simultaneously during evaluation. Although modern VLMs like GPT-4o [67] are highly capable, their **cross-image attention remains limited**. When too many images are provided, the model struggles to accurately perceive each image’s content, leading to unreliable assessments of composition quality and consequently wrong scores, as illustrated in first row of Fig. 5.

4.2. Weighted-Ref-VIEScore

To overcome the limitations of existing evaluation frameworks, we introduce a weighted, reference-based evaluation

paradigm tailored for multi-image composition.

Weighting: During each evaluation, every non-human source image is first paired with the generated result and fed into Qwen-VL2.5-72B [3] to determine whether the source image successfully appears in the generated output. For facial source images, we instead employ ArcFace [21] to verify whether the corresponding face is correctly preserved in the result. This process yields a weight for each source image, reflecting its contribution to the composition. However, relying solely on these weights may be exploited by models, for instance, **by trivially copy-pasting all sources into the output**. To prevent such bias, we incorporate a complementary reference-based mechanism.

Reference: For each case, we first generate a high-quality reference image using Nano-Banana [18], followed by rigorous human verification to ensure that all source elements are faithfully represented, with the necessary visual variance and semantic alignment with the given prompt. During evaluation, GPT-4o [67] compares each generated image with its reference image individually, rather than jointly processing all source images, as illustrated in Fig. 5 (Weighted-Ref-VIEScore). This design yields a more accurate and human-aligned SC score. The PQ score is then computed solely based on the generated image. Finally, the overall score is defined as $W \times \sqrt{SR \times PF} \times PQ$ where

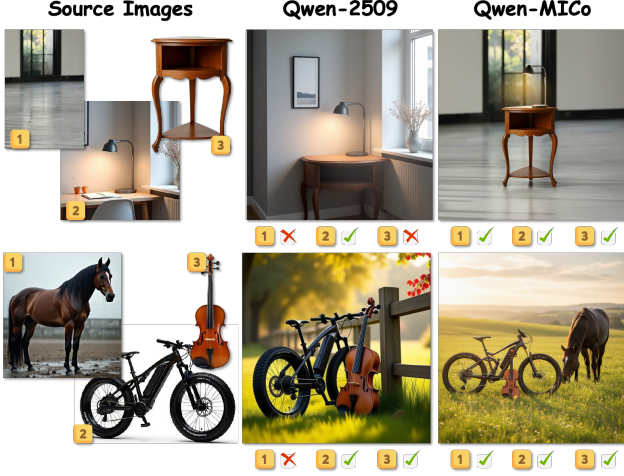


Figure 6. Qwen-Image-2509 is trained on a massive-scale dataset and supports only three-image inputs, while Qwen-MiCo is trained solely on MiCo-150K and supports arbitrary multi-image inputs, producing images with higher aesthetic quality.

W denotes the source-specific weighting factor. Extensive user studies demonstrate that our metric aligns with human preference significantly better than existing alternatives.

A more detailed computation procedure is provided in Sec. 7.4. The human study validating the Weighted-Ref-VIEScore is presented in Sec. 7.5. Additional ablation studies, including *Reference Image and Style Homology Risk*, *GPT-4o Evaluator-Generator Coupling*, and *Resistance to Copy-Paste Attacks*, are discussed in Sec. 7.6.

4.3. Benchmark Curation

We construct MiCo-Bench by selecting 200, 200, and 300 representative cases from the Object-Centric, Person-Centric, and Human-Object Interaction tasks of MiCo-150K (as shown in Tab. 1), respectively—100 cases from each sub-task, and an additional 300 cases from the De&Re subset, resulting in 1,000 high-quality benchmark cases. To ensure annotation reliability and fairness, we invited three independent reviewers who were not involved in this project to perform the selection. These reviewers were unaware of the distinctions between the general composition tasks and the De&Re task. Each case was evaluated from two perspectives: (1) whether all objects from the source images were correctly preserved in the generated result, and (2) whether the final image aligned with the textual instruction. Only the cases unanimously judged as satisfactory by all three reviewers were retained for the final benchmark.

5. Experiments

5.1. Experiments Setting

To validate the effectiveness of our dataset, we train five open-source models: BAGEL [19], OmniGen2 [84], Luminia-DiMOO [89], BLIP3-o [12], Qwen-Image-Edit [83] on MiCo-150K, and evaluate their performance on MiCo-Bench. For BAGEL, we freeze the understanding branch and VAE while fine-tuning the generation branch parameters. For BLIP3-o, we build upon the BLIP3o-Next-Edit [13] version and set the maximum sequence length to 5120, with sequences right-padded or truncated as needed. For OmniGen2, we simply perform full fine-tuning. For Luminia-DiMOO, we set the input maximum sequence length to 6144, and resize all input images to 512×512 . For Qwen-Image-Edit, we use our custom training pipeline. The encoder and VAE are frozen, while all parameters of the MMDiT module are fine-tuned. We further conducted an ablation study on the De&Re task, comparing three training configurations: without De&Re, with real De&Re target images, and with synthetic De&Re target images.

5.2. Results and Discussions

The experimental results in Tab. 2 show that, after fine-tuning on MiCo-150K, all models with diverse architectures and initial capabilities exhibit substantial improvements in multi-image composition. Notably, our baseline model, the fine-tuned **Qwen-MiCo** (derived from Qwen-Image-Edit [83]) achieves performance close to that of closed-source models, further demonstrating the effectiveness of our dataset. Further quantitative experiments and qualitative examples of Qwen-MiCo are provided in Sec. 7.7.

Open-Source Models. As shown in Fig. 7, BLIP3-o and DiMOO, which originally lack any MiCo ability, exhibit clear gains after fine-tuning on MiCo-150K. BAGEL and Qwen-Image-Edit, benefiting from large-scale multi-task pretraining, already display *emergent MiCo capabilities*, which are further reinforced after fine-tuning. The fine-tuned Qwen-MiCo achieves 3-image composition performance comparable to Qwen-Image-2509 [57], as shown in Fig. 6, despite the latter being trained on a dataset hundreds of times larger. Moreover, Qwen-MiCo supports arbitrary multi-image inputs, whereas Qwen-Image-2509 is limited to three. OmniGen2, pretrained on MiCo-related tasks, already exhibits compositional ability, especially in maintaining facial identity, and further benefits from MiCo-150K.

Closed-Source Models. Overall, Nano-Banana achieves higher quantitative scores, yet GPT-4o exhibits superior robustness. Regardless of the input configuration, GPT-4o consistently produces coherent and semantically appropriate compositions, avoiding issues such as incomplete bodies, total identity loss, or direct “copy-paste” artifacts that occasionally appear in Nano-Banana’s outputs. Represen-

Table 2. Performance comparison on MICO-Bench across different open-source and closed-source model: “base” denotes the original model; “w/o” indicates fine-tuning without the De&Re task; “real” and “synth” correspond to fine-tuning with real and synthetic compositions from the De&Re task, respectively. The best performance of each model under each task is highlighted in **bold**.

Model	Overall				Object				Person				HOI				De&Re			
	base	w/o	real	synth	base	w/o	real	synth	base	w/o	real	synth	base	w/o	real	synth	base	w/o	real	synth
<i>Open-Source Models</i>																				
BLIP3-o	2.2	42.2	43.2	43.0	3.2	36.7	36.7	36.6	2.1	41.2	41.3	41.3	2.1	45.6	46.7	46.6	1.2	42.1	45.2	45.1
DiMOO	4.3	32.3	34.2	33.9	3.8	33.8	33.8	33.6	1.3	31.6	31.7	31.6	6.5	39.5	40.1	40.2	1.8	23.9	27.0	26.7
BAGEL	33.3	42.6	44.3	44.1	31.4	39.3	39.3	39.2	32.4	44.6	44.8	44.6	26.9	38.0	38.9	38.9	41.2	48.1	50.9	50.6
Qwen-Image	38.5	56.4	58.2	58.1	35.4	53.0	53.1	53.0	38.8	56.4	56.6	56.5	36.9	56.5	56.9	56.8	41.4	58.2	60.7	60.6
OmniGen2	41.0	50.6	51.2	50.7	39.0	42.1	42.2	42.1	33.1	50.1	50.4	50.2	39.5	54.4	54.8	54.8	46.9	51.9	52.4	52.3
<i>Closed-Source Models</i>																				
GPT-4o	59.6	–	–	–	59.1	–	–	–	53.8	–	–	–	60.1	–	–	–	61.3	–	–	–
Nano-Banana	60.3	–	–	–	58.6	–	–	–	59.4	–	–	–	62.1	–	–	–	60.4	–	–	–



Figure 7. The leftmost displays the source and reference images. The first row shows model outputs before fine-tuning, the second row presents outputs after fine-tuning. The Weighted-Ref-VIEScore for each generated result is annotated in the corner. MICO-150K demonstrates strong robustness: **BLIP-3o** and **Lumina-DiMOO** acquire MICO capability from scratch; the emergent MICO abilities of **BAGEL** and **Qwen-Image** are significantly strengthened; **OmniGen2** achieves further improvement on top of its already strong performance.

tative cases are illustrated in Fig. 9 of the Appendix.

Emergent Capability. It is worth noting that BAGEL and Qwen-Image-Edit were not trained on any multi-image composition data. However, *when multiple source image tokens are simply concatenated and fed into the model, they exhibit emergent MICO ability*. After simple SFT on MICO-150K, these abilities are significantly enhanced. Moreover, even without using data from the De&Re task, where no other training samples contain combined human, object, clothing, and scene all together, all models still demonstrate emergent performance on the MICO-Bench De&Re subset.

Synthetic Data vs. Real Data. Each group of source images in the **De&Re** task is paired with a real and a synthetic target. As shown in Tab. 2, models trained on synthetic targets achieve nearly identical performance to those trained on real ones, showing that carefully curated synthetic data

can serve as an effective substitute in MICO training.

6. Conclusion

We introduced the **Multi-Image Composition (MICO)** task, along with **MICO-150K**, the first large-scale high-quality dataset tailored for this task. MICO-150K encompassed three tasks, seven subtasks, and 27 composition types, along with a **De&Re** subset providing real–synthetic pairs for controlled comparison, totaling 150K MICO cases with varying numbers of input images. We further proposed **MICO-Bench** and **Weighted-Ref-VIEScore**, providing a reliable framework for evaluating MICO performance. Extensive experiments revealed interesting insights and showed that finetuning on MICO-150K could consistently boost the MICO performance of different models with different initial capability. Notably, our baseline model

Qwen-MiCo achieved 3-image composition performance comparable to Qwen-Image-2509, which was trained on a dataset hundreds of times larger. However, Qwen-Image-2509 was restricted to 3-image inputs, while Qwen-MiCo supported a larger number of input images.

7. Appendix

We organize this **Appendix** into the following sections:

- **A1. Reproducibility, Licensing, Data Release**
- **A2. Visualizations and Qualitative Examples**
- **A3. Analysis of Human-Face Source Images**
- **A4. Details of Weighted-Ref-VIEScore**
- **A5. Human Study and Metric Alignment**
- **A6. Additional Experiments**
- **A7. Quantitative Evaluation of Qwen-MiCo**

7.1. Reproducibility, Licensing, Data Release

MiCo-150K and MiCo-Bench (which are strictly non-overlapping—the training set contains no MiCo-Bench images) will be fully released upon acceptance. The release will include all source images (or corresponding metadata), all multi-image composition tasks, and the complete set of GPT-based evaluation prompts. All GPT evaluations in the main paper were conducted with `temperature=0`, yielding deterministic outputs and ensuring full reproducibility.

All MiCo-150K source images come from publicly released datasets with open licenses, including Subject200k [66], VITON-HD [15], X2I-Subject-Driven [88], Mulan [72], Echo-4o [93], SUN397 [87], and CC12M [8]. The two headshot datasets used for identity filtering, BKM1804/headshot_istockphoto [4] and BKM1804/headshot_pexels_v1 [5], are released under the **Creative Commons Attribution 4.0 (CC BY 4.0) license**. This license permits redistribution, modification, and research use, provided that proper attribution is given.

Our use of these datasets conforms to all licensing and redistribution requirements. No private or restricted data were used, and no personally identifiable images outside openly licensed sources were collected.

7.2. Visualizations and Qualitative Examples

We provide additional visual examples. Fig. 8 illustrates examples from the five open-source models before and after being trained on MiCo-150K. Fig. 9 compares examples generated by GPT-Image-1 [51] and Nano-Banana [18].

7.3. Analysis of Human-Face Source Images

7.3.1. Data Sources, Licensing, and Ethics

Celebrity Faces. All celebrity portraits in MiCo-150K originate exclusively from the public X2I-Subject-Driven dataset [88], which provides high-quality subject-centric

photographs under a research-permissive license. No additional celebrity images were crawled or collected from the web. To mitigate right-of-publicity and privacy risks, **raw celebrity images will not be redistributed**; only derived metadata and selection indices will be released.

Non-Celebrity Faces. The remaining portraits are drawn from three established datasets commonly used in virtual try-on and portrait-generation research: VITON-HD [15] (research-only license), Headshot iStockPhoto [4] and Headshot Pexels v1 [5] (CC-BY-4.0). The two headshot datasets released under **CC-BY-4.0** explicitly permit redistribution, modification, and research use with proper attribution, as discussed in Sec. 7.1. All images were used in strict accordance with their respective licenses.

Across all sources, MiCo-150K contains **no private, scraped, or user-uploaded photographs**. The portraits are used solely for constructing multi-image composition tasks; no identity recognition, biometric profiling, or sensitive attribute inference is performed.

7.3.2. Demographic Distribution Analysis

To understand the demographic characteristics and potential bias of the human-face source images used in MiCo-150K, we employed **Qwen2.5-VL-72B** to estimate three attributes for each portrait: (1) ethnicity, (2) gender, and (3) coarse age group. In total, we analyzed **53,648** human-face source images, including **11,677** images used in the De&Re task and **41,971** images used in all other MiCo tasks.

Ethnicity. The estimated ethnic distribution is *East/Southeast Asian: 6,740, South Asian: 3,337, European/Middle Eastern: 33,982, African: 9,290 and Others: 299*. This reveals an over-representation of European/Middle Eastern subjects and relative under-representation of Asian groups, reflecting the typical skew of widely used portrait datasets.

Gender. The raw gender distribution is *Male: 21,241 and Female: 32,407*. During MiCo-150K task construction, however, we explicitly enforced gender balancing. Across the 159,091 human-face images sampled for all compositions (see Tab. 1 in the main paper), the resulting ratio becomes approximately 1:1, mitigating upstream imbalance.

Age. The age distribution is *Child: 1,421, Teen/Young Adult: 31,413, Middle-Aged: 19,146, and Older Adult: 1,668*, showing a strong dominance of young adults, a pattern that is common in fashion, try-on, and aesthetic portrait datasets. Importantly, for multi-image composition tasks, this age skew is unlikely to negatively impact model behavior, as real-world applications naturally exhibit a similar young-adult majority. Thus, while the distribution is uneven, it is largely aligned with practical usage scenarios.

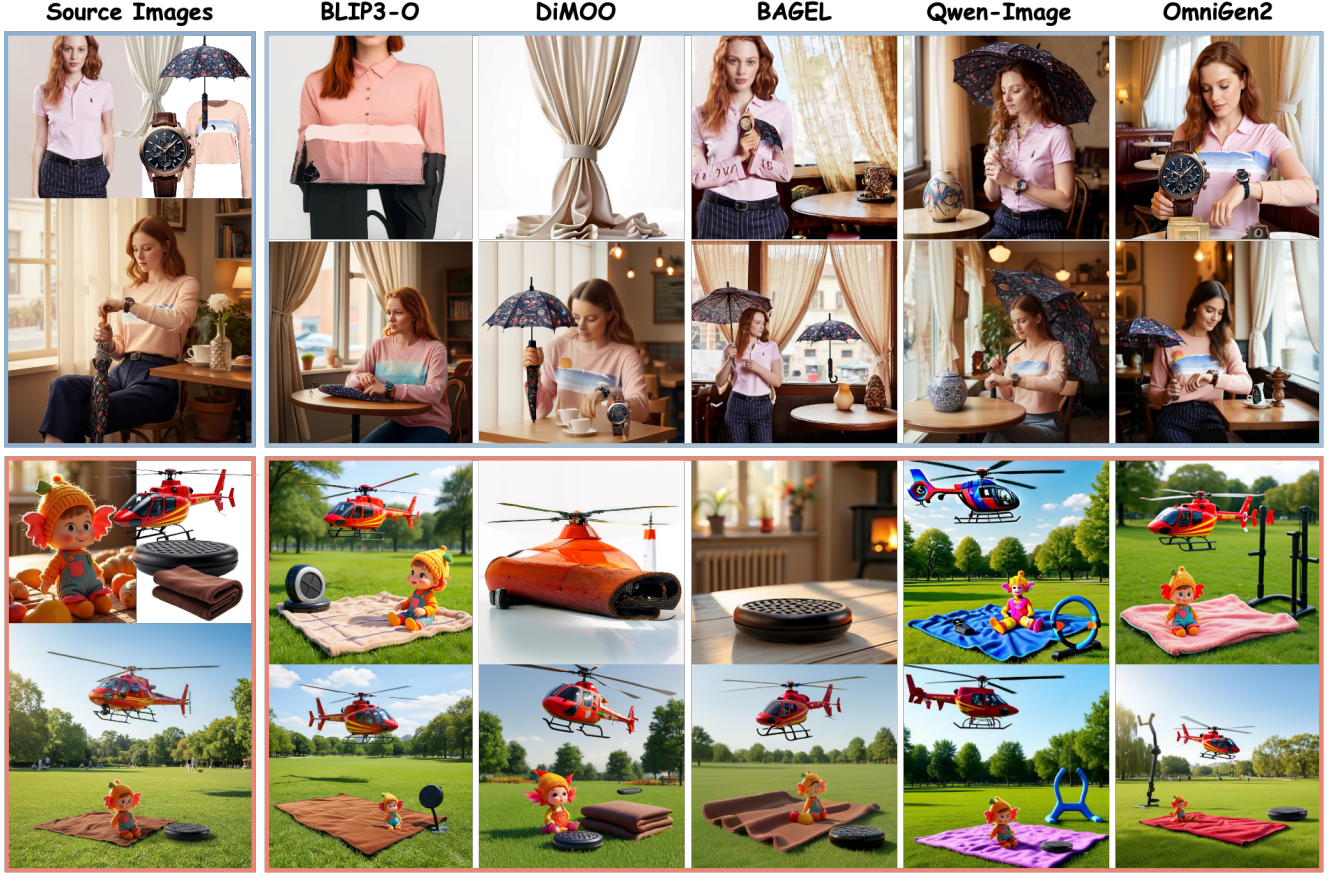


Figure 8. Comparison of open-source models before and after MICo-150K training. Some source images were cropped or background-removed for visualization. BLIP3-o [12] and Luminia-DiMOO [89] gain strong multi-image composition abilities after training. Qwen-Image-Edit [83] and BAGEL [19] were not explicitly trained for MICo tasks, but exhibit emergent MICo capabilities that are further enhanced through fine-tuning. OmniGen2 [84] preserves identity well and produces more aesthetic, prompt-aligned results after training.

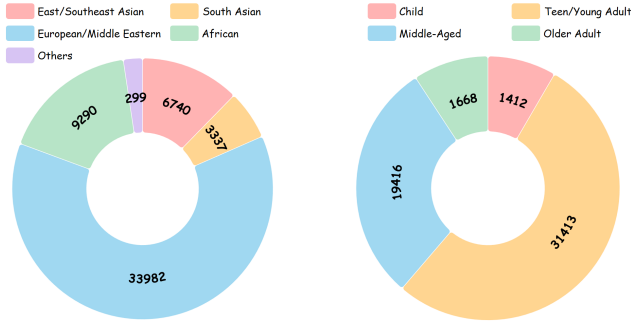


Figure 10. Human-face source images exhibit a Western-centric ethnicity skew and a young-adult bias, reflecting characteristics inherent in the upstream public datasets rather than biases introduced by MICo-150K itself.

Discussion and Mitigation. The demographic analysis highlights several imbalances, particularly a Western-centric ethnicity skew and a young-adult bias. These limitations stem from upstream public datasets and are not spe-

cific to MICo-150K. We emphasize that MICo-150K is **not designed** for fairness benchmarking or identity-sensitive evaluations. Instead, its purpose is restricted to studying visual multi-image composition.

Overall, while demographic skew is present, as shown in Fig 10, we openly document these statistics to facilitate informed and responsible use. We caution against applying MICo-150K in fairness-critical or identity-sensitive contexts. Future work may incorporate more diverse portrait sources to improve global representativeness.

7.4. Details of Weighted-Ref-VIEScore

7.4.1. Weights

As described in Sec. 4.2 of the main paper, the Weighted-Ref-VIEScore applies a multiplicative visibility coefficient W , computed as the ratio between (i) the number of source images whose key content is successfully preserved in the generated target image and (ii) the total number of source images. The critical step is therefore determining whether a

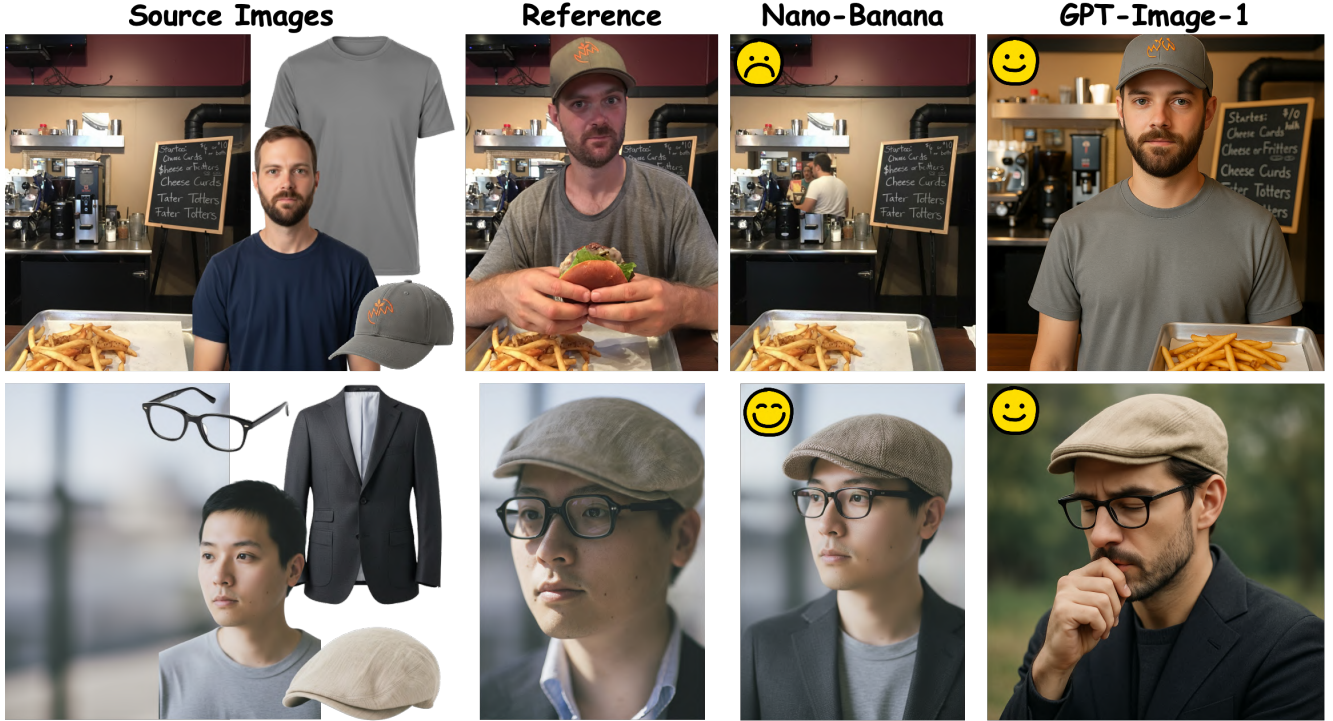


Figure 9. Nano-Banana [18] produces more realistic images with stronger fidelity to the source inputs and a higher quality ceiling, but occasionally fails on certain cases. GPT-Image-1 [51] exhibits a more stylized, less photo-realistic look, yet remains highly stable and consistently yields semantically coherent results.

source element is present in the target image.

Objects, clothing items, and scenes. For non-human content, we employ Qwen2.5-VL-72B [3] to compare the source and target images. For each case, we construct a task-specific binary question (e.g., “Does the <object> in the source image appear in the target image?”) and treat the model’s answer as a binary indicator of presence.

Human faces. For source images containing faces, we use ArcFace [21] to extract identity embeddings from both source and target portraits and compute cosine similarity. According to the finding in [90], face-ID similarity is *not* a “higher-is-better” metric: extremely high similarity often indicates copy–paste artifacts and leads to unnaturally rigid identity transfer. Real photos of the same person typically form a similarity distribution peaking around ~ 0.58 , rather than near 1.0. To balance identity consistency with realism, we use task-dependent thresholds: identity is treated as preserved when the similarity exceeds *0.50 for person-centric tasks*; and *0.45 for all other tasks*, where facial details are less essential. These thresholds prevent the metric from favoring trivial copy–paste solutions while still recognizing correct identity transfer in multi-image composition.

7.4.2. SC and PQ Scoring

To compute the Semantic Consistency (SC) and Perceptual Quality (PQ) components of the Weighted-Ref-VIEScore, we query GPT-4o twice, once for SC and once for PQ.

For SC scoring, although current general-purpose VLMs [1, 2, 40, 41, 43, 46, 69, 73, 74, 96] are very powerful, they still struggle to perform reliable cross-image attention. Therefore, we use only a single reference image. Specifically, the model takes two images as input, a reference image and the image to be evaluated, and outputs two sub-scores:

- **Prompt Following (PF):** how well the generated image follows the textual input prompt;
- **Subject Resemblance (SR):** how well the generated image matches the reference image in terms of people, scenes, clothing, and objects.

Both PF and SR are scored on a $[0, 10]$ scale, and the final SC score is defined as $SC = \sqrt{SR \times PF}$. We use a fixed meta-prompt for SC evaluation. The full prompt template is provided in our fully open-source [repo](#).

For PQ scoring, the model takes only the image to be evaluated as input and produces two sub-scores:

- **Naturalness:** evaluates whether the generated image appears visually plausible, including coherent lighting, shadows, geometry, and overall realism.

- **Artifacts:** measures the absence of visual defects such as distortions, duplicated limbs, or unnatural textures.

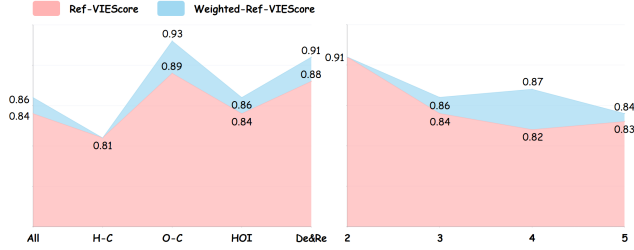


Figure 11. We refer to the metric without the weighting factor W as **Ref-VIEScore**. We conduct extensive human studies and compute the *Spearman rank correlation* between human preferences and the rankings produced by both **Weighted-Ref-VIEScore** and **Ref-VIEScore**. The results are summarized in the figure.

Both naturalness and artifacts are scored on a [0,10] scale, and the final PQ score is defined as their geometric mean. The full prompt template is in our open-source [repo](#).

7.5. Human Study and Metric Alignment

To validate the effectiveness of Weighted-Ref-VIEScore, we conducted an extensive human study to measure its alignment with human preferences. From the 27 task types in MICO-Bench, we sampled two cases per type, and additionally selected 21 cases from the De&Re task, yielding a total of 75 evaluation cases.

For each case, we randomly selected five candidate outputs from a pool of twelve models: five open-source models (BLIP-3o [12], Lumina-DiMOO [89], BAGEL [19], Qwen-Image-Edit [83], OmniGen2 [84]) in both their pre-training and MICO-finetuned versions, and two closed-source models (GPT-Image-1 [51] and Nano-Banana [18]). Human evaluators were provided with the *source images*, *text prompts*, and the *five anonymized candidate outputs* for ranking.

We recruited 25 human participants, all holding at least a bachelor’s degree, including 9 senior Ph.D. students. We further define Ref-VIEScore as the variant of our metric *without* the weighting factor W , i.e., $SC \times PQ$.

For each case, we computed the **Spearman rank correlation** between each participant’s ranking and the rankings produced by Weighted-Ref-VIEScore and Ref-VIEScore. The average correlation across 25 participants was used as the final correlation score for that case. We report results under two groupings: (1) grouped by **task type**, and (2) grouped by the **number of input source images**. The results, summarized in Fig. 11, reveal three key findings:

1. **Strong human-metric alignment.** Weighted-Ref-VIEScore achieves consistently high Spearman correlations across all task types, indicating robust agreement with human judgment.

2. **Robustness to varying numbers of source images.** Thanks to our reference-image design, Weighted-Ref-VIEScore maintains stable accuracy regardless of how many source images are provided as input.
3. **Importance of the weighting factor W .** Weighted-Ref-VIEScore outperforms Ref-VIEScore across all settings. Moreover, the inclusion of W provides interpretability by revealing which source elements failed to appear in the generated image, a capability essential for diagnosing and improving model behavior.

7.6. Additional Experiments

7.6.1. Reference Image and Style Homology Risk

A natural concern is whether Weighted-Ref-VIEScore may implicitly favor images whose visual style is closer to that of the reference generator, since reference images for most MICO-Bench tasks are synthesized using Nano-Banana [18]. One might hypothesize that models producing Nano-Banana-like aesthetics could receive higher scores.

We first clarify the setup: for all De&Re task cases, the reference images are real photographs, whereas only the reference images for the remaining 27 task types are generated by Nano-Banana.

To evaluate whether such style homology affects scoring, we randomly sampled **108 cases** from the non-De&Re task types (4 cases per type). For each case, we generated outputs from three different models, GPT-Image-1 [51], Qwen-MICO, and Nano-Banana [18]. We then computed a style distance between each model output and the corresponding reference image using DINOv2 [52] ViT-b cosine distance, a strong self-supervised perceptual feature encoder widely used for measuring cross-image similarity.

This produced a sequence of model rankings induced by style distance and a sequence of rankings induced by Weighted-Ref-VIEScore. We computed the Spearman correlation ρ between these two rankings for each case.

Across all 108 cases, the mean correlation was $\rho = 0.251$, indicating only a weak association between reference-style similarity and VIEScore ranking. In other words, models whose outputs resemble the Nano-Banana reference style are **not** systematically favored. Weighted-Ref-VIEScore does **not** reward stylistic imitation, and its scoring behavior is largely orthogonal to reference similarity. Qualitative examples illustrating this lack of dependency are shown in Fig. 12.

7.6.2. GPT-4o Evaluator-Generator Coupling

Since our evaluation relies on GPT-4o [67] to compute both the **PQ** (Perceptual Quality) and **SC** (Semantic Consistency) scores, a natural concern is the potential risk of *evaluator-generator coupling*: if a generative model produces images whose style is similar to that of GPT-Image-1 [51] (or when GPT-Image-1 itself is being evaluated), could such

Table 3. We evaluate on the MICO-Bench subset where each case contains exactly three input images, since Qwen-Image-2509 does not support higher-order composition. Qwen-MiCo consistently outperforms Qwen-Image-2509 across nearly all evaluation dimensions.

Method	Object Centric		Person Centric					HOI			
	201S	3O	2M1W	2W1M	3M	3W	2P1S	1P2O	2P1O	1P2C	1P1C1O
Qwen-MiCo	56.12	59.56	59.04	58.96	50.11	56.19	60.97	54.92	52.16	55.82	54.26
Qwen-Image-2509	56.00	45.32	42.63	52.46	48.40	50.78	49.70	50.64	54.65	51.77	47.91



Figure 12. Similarity to the reference image does not influence how Weighted-Ref-VIEScore ranks model outputs, demonstrating that the metric remains objective and well-aligned with human preferences.

outputs receive artificially inflated scores? Although prior works [27, 30, 79, 82] suggest that GPT-based evaluators do *not* inherently favor GPT-generated content, we explicitly examine this possibility in the MICO evaluation setting.

Following the procedure in Sec. 7.6.1, we sampled the same 108 non-De&Re cases from MICO-Bench and obtained outputs from three models: GPT-Image-1 [51], Qwen-MiCo, and Nano-Banana [18]. For each case, we computed a style distance by measuring the DINOv2 feature distance between each model’s output and the output generated by GPT-Image-1 for the same case.

We then computed the correlation between this style-distance sequence and three evaluation-score sequences: SC scores, PQ scores, and Ref-VIEScore ($SC \times PQ$). The resulting Spearman correlations were: $\rho_{SC} =$

-0.115 , $\rho_{PQ} = -0.008$, $\rho_{\text{Ref-VIEScore}} = -0.077$.

All correlations are near zero, indicating that neither SC, PQ, nor Ref-VIEScore favors outputs stylistically closer to GPT-generated images, even though GPT-4o is used as the evaluator. This confirms the absence of evaluator-generator coupling in the MICO evaluation setting. Representative qualitative examples are shown in Fig. 13.

7.6.3. Resistance to Copy-Paste Hack

A common failure mode for composition models is the *copy-paste hack*: directly cutting objects or faces from the source images and pasting them onto a new background. An effective metric must not reward such behavior.

To test whether Weighted-Ref-VIEScore can be fooled by this shortcut, we constructed explicit copy-paste baselines. For two representative sub-tasks, **Object+Scene** and

Reference		Qwen-MICo		GPT-Image-1		Nano-Banana	
							
DinoV2	Ref-VIES	0.362	72.00	1.000	51.85	0.776	76.37
PQ Score	SC Score	9.00	8.00	8.00	6.48	9.00	8.49
Spearman Correlation= -0.50 !		Spearman Correlation= -0.87 !		Spearman Correlation= -0.50 !			
							
DinoV2	Ref-VIES	0.756	80.50	1.000	80.50	0.616	90.00
PQ Score	SC Score	9.49	8.49	9.49	8.49	9.49	9.49
Spearman Correlation= -0.87 !		Spearman Correlation= 0.00 !		Spearman Correlation= -0.87 !			

Figure 13. Although PQ and SC scores are computed using GPT-4o, we find no evidence of evaluator-generator coupling: images that are stylistically closer to GPT-Image-1 do *not* receive higher scores. The evaluation depends solely on MICo output quality and remains well aligned with human preferences.

Person+Scene, we randomly sampled 10 cases each. For every case, we segmented the source objects (or person) using an off-the-shelf segmentation tool [58] and manually pasted them onto the scene image, creating a naive composite without any harmonization.

Although these copy-paste outputs achieve a perfect weight factor $W = 1.00$ (since all source elements appear in the target), their **PQ** and **SC** scores are extremely low. Across all 20 constructed cases, the final Weighted-Ref-VIEScore averages only **14.16**, demonstrating that the metric effectively penalizes unnatural compositing and cannot be exploited by trivial cut-and-paste strategies. Representative examples are shown in Fig. 14.

7.7. Quantitative Evaluation of Qwen-MICo

For fair comparison, we clarify that Qwen-Image-2509 [57] was released before MICo-150K became available, and thus it could not have used our dataset for training. This eliminates the possibility of data leakage or overlap between MICo-150K and Qwen-Image-2509’s training corpus.

To further quantify the performance gap between Qwen-Image-2509 [57] and Qwen-MICo, we evaluate both models on the subset of MICo-Bench containing tasks with exactly three input images (see Tab. 1 in the main paper). This subset includes 11 task types, *2OIS*, *3O*, *2MIW*, *2WIM*, *3M*, *3W*, *2PIS*, *1P2O*, *2P1O*, *1P2C*, *1P1C1O*. For each type, we randomly sample five cases, yielding a total of 55 evaluation instances. We then compute the proposed Weighted-Ref-VIEScore for both models across all cases.

As reported in Tab 3, Qwen-MICo consistently outperforms Qwen-Image-2509 across nearly all evaluation dimensions, despite using two to three orders of magnitude less training data and supporting arbitrary numbers of input images, whereas Qwen-Image-2509 is limited to three-image composition. Additional qualitative comparisons are shown in Fig. 15, illustrating the superior compositional fidelity and visual coherence achieved by Qwen-MICo.

In addition, we observe that Qwen-MICo exhibits several remarkable emergent capabilities, with representative examples shown in Fig. 16–Fig. 20.



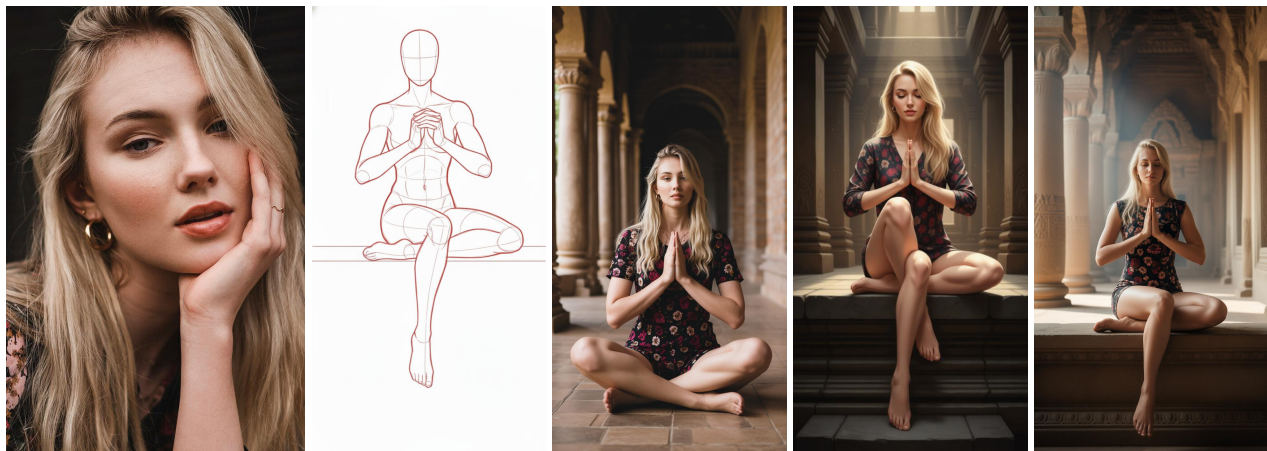
Figure 14. Weighted-Ref-VIEScore effectively **prevents copy-paste hacks**. We segmented objects or persons from the source images and manually pasted them onto the scene image to form a naïve, unharmonized composite. Although such copy-paste results achieve a perfect weight factor (since every source element appears in the output), their PQ and SC scores remain very low.



Figure 15. Qwen-MiCo consistently outperforms Qwen-Image-2509 across nearly all evaluation dimensions on the MiCo-Bench three-image subset. While Qwen-Image-2509 is trained on a massive corpus but restricted to three-image inputs, Qwen-MiCo—trained only on MiCo-150K—supports arbitrary multi-image composition and yields higher compositional fidelity and visual quality.



Prompt: The man from image 1 is doing the pose from image 2. He is leaning casually on a railing or balcony. His weight rests on his straight left leg, with his right knee bent and the foot resting on the inside of his standing leg. His left arm is relaxed, gripping the rail for support. The right hand is raised to his face, touching his chin in a thoughtful or contemplative gesture. This pose conveys a sense of relaxed elegance and pause. The scene is set against a vibrant city street during the warm hues of dusk, suggesting a moment of quiet reflection.



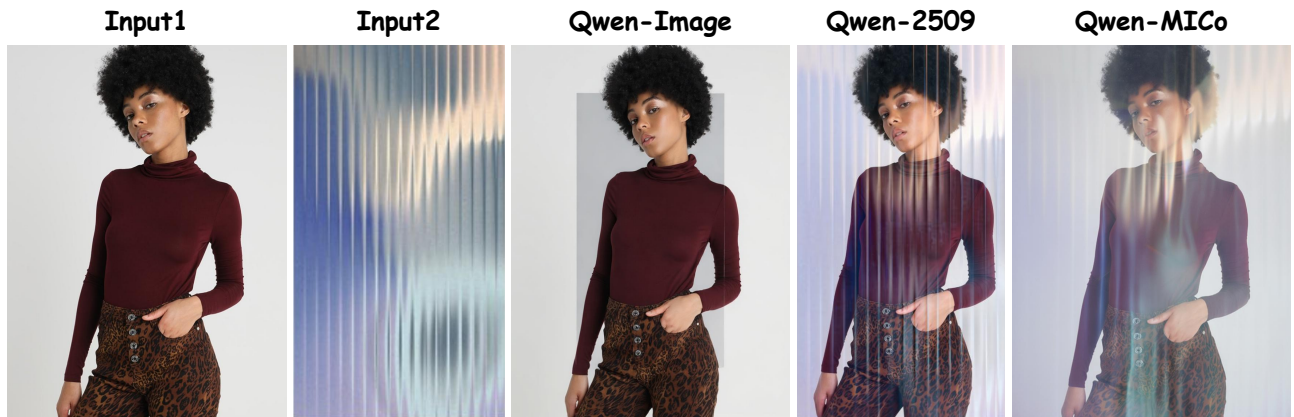
Prompt: The girl from image 1 is doing the pose from image 2. She is seated in a calm, centered pose, suggesting deep contemplation or meditation. She is sitting on an elevated surface with her left leg crossed and tucked towards her body, while her right leg hangs down vertically. Her hands are clasped together at chest level in a prayer-like or focused gesture. The pose is very stable and symmetrical, conveying serenity and quiet focus. This tranquil scene unfolds within the peaceful confines of an ancient temple, where soft, diffused light filters through the grand architecture, enhancing the sense of spiritual quietude.

Figure 16. Qwen-MICo exhibits strong emergent abilities in recognizing and composing complex **human poses**.



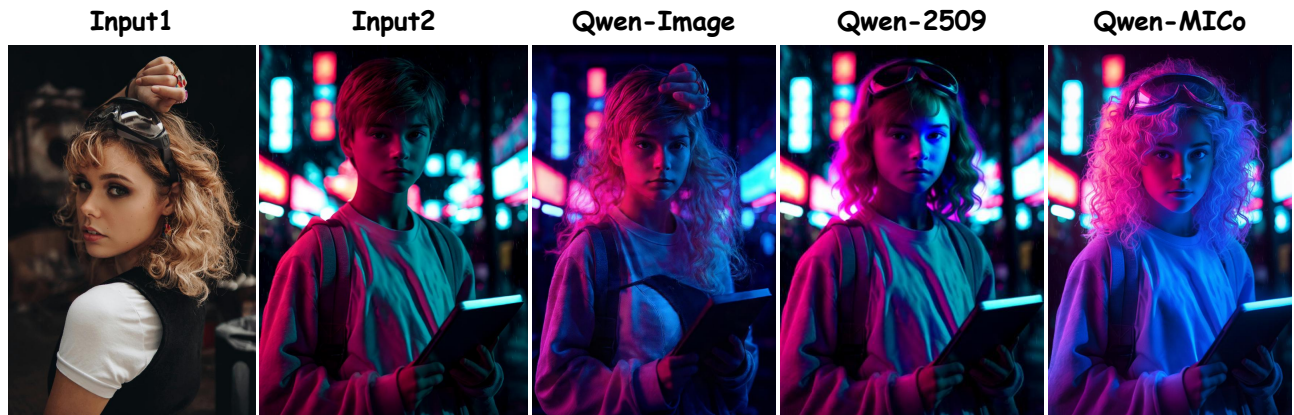
Prompt: The girl from image 1, with her striking red hair, is now adorned with the elaborate makeup from image 2. Her eyes feature lightly applied purple and black eyeshadow, accented by glitter and star-shaped appliqués, creating a bold, artistic look. A lip piercing, a pendant earring, star-sticker on the hair, and pearl-necklace with a floral motif complete her transformation, presenting her in a striking, avant-garde style that contrasts beautifully with her natural features.

Figure 17. Qwen-MICo performs well on **virtual makeup try-on** (transferring the makeup in Image 2 onto the girl in Image 1).



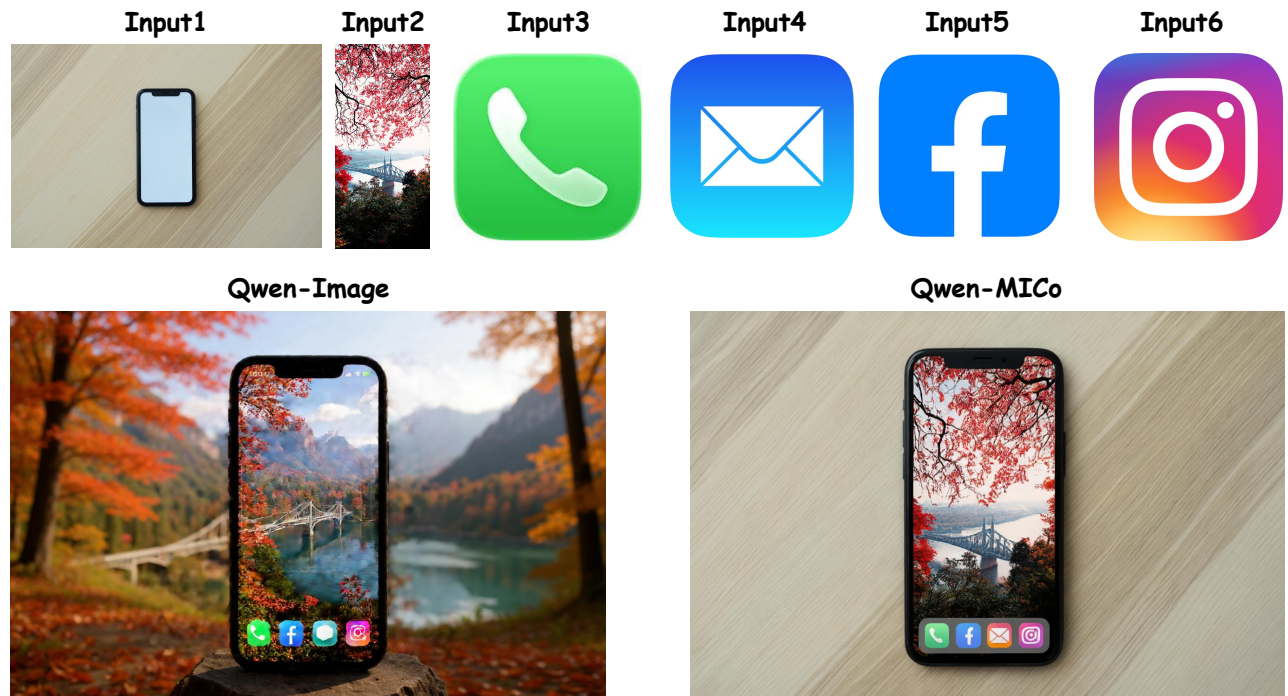
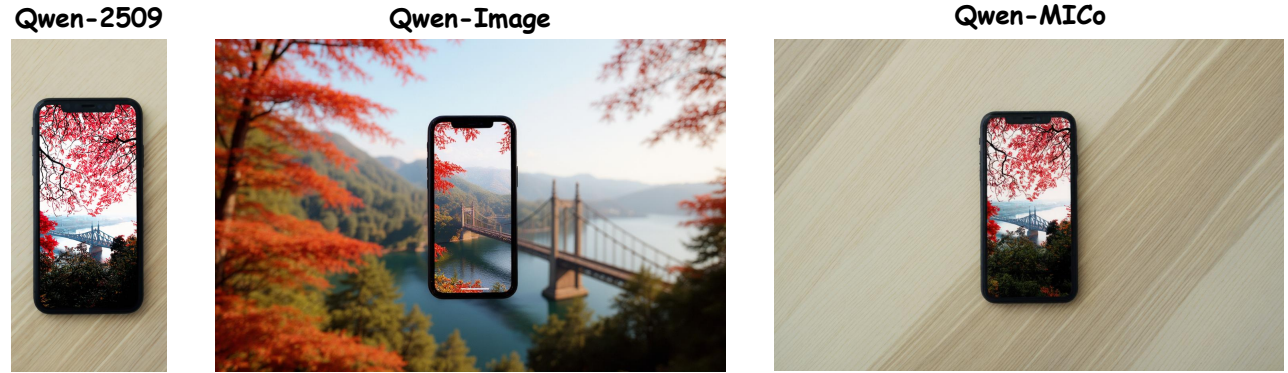
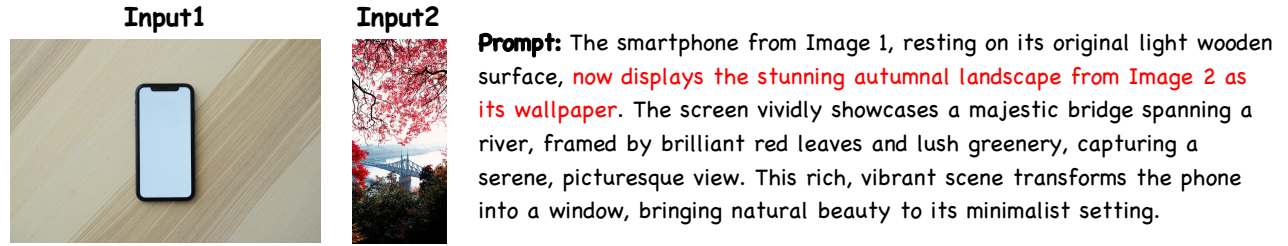
Prompt: Overlay the shimmering, ethereal glass effect from Image 2 onto the photo in Image 1. This transformation will introduce a layer of transparent distortion and refracted light, giving the original image a dreamlike, almost liquid quality. The effect should subtly bend and fragment the underlying visuals, creating an artistic and surreal interpretation that captivates the viewer.

Figure 18. Qwen-MICo shows excellent performance on visually complex tasks that demand a **deep understanding of lighting and optics**, and produces outputs with strong aesthetic appeal.



Prompt: The woman from image 1, with her curious gaze and goggles pushed up, is now bathed in the intense, neon-drenched cyberpunk lighting from image 2. Her curly blonde hair and expressive face are dramatically highlighted by vibrant cyan and magenta hues, casting a futuristic glow upon her while her original dark, workshop-like background remains. This striking contrast creates a captivating visual, blending her grounded essence with an electric, dystopian ambiance.

Figure 19. Qwen-MICo preserves the subject's identity while accurately modeling **lighting and shading**, transferring the illumination from Image 2 onto the girl in Image 1.



Prompt: The smartphone from Image 1, resting on its original light wooden surface, now displays the stunning autumnal landscape from Image 2 as its wallpaper. The screen vividly showcases a majestic bridge spanning a river, framed by brilliant red leaves and lush greenery, capturing a serene, picturesque view. Neatly arranged at the very bottom of the phone's screen are the application icons for phone calls from image 3, Mails from image 4, Facebook from image 5, and Instagram from image 6. This rich, vibrant scene transforms the phone into a window, bringing natural beauty to its minimalist setting.

Figure 20. Qwen-MICo preserves the entire appearance of Input 2 while correctly interpreting the prompt phrase “resting on its original light wooden surface”. On top of this, it supports more image inputs than Qwen-Image-2509, and accurately renders all application icons onto the phone’s home screen.

References

- [1] Ruichuan An, Sihan Yang, Ming Lu, Renrui Zhang, Kai Zeng, Yulin Luo, Jiajun Cao, Hao Liang, Ying Chen, Qi She, et al. Mc-llava: Multi-concept personalized vision-language model. *arXiv preprint arXiv:2411.11706*, 2024. 12
- [2] Ruichuan An, Sihan Yang, Renrui Zhang, Zijun Shen, Ming Lu, Gaole Dai, Hao Liang, Ziyu Guo, Shilin Yan, Yulin Luo, et al. Unictokens: Boosting personalized understanding and generation via unified concept tokens. *arXiv preprint arXiv:2505.14671*, 2025. 12
- [3] Shuai Bai, Keqin Chen, Xuejing Liu, Jialin Wang, Wenbin Ge, Sibao Song, Kai Dang, Peng Wang, Shijie Wang, Jun Tang, Humen Zhong, Yuanzhi Zhu, Mingkun Yang, Zhaohai Li, Jianqiang Wan, Pengfei Wang, Wei Ding, Zheren Fu, Yiheng Xu, Jiabo Ye, Xi Zhang, Tianbao Xie, Zesen Cheng, Hang Zhang, Zhibo Yang, Haiyang Xu, and Junyang Lin. Qwen2.5-vl technical report, 2025. 3, 4, 7, 12
- [4] BKM1804. headshot_istockphoto: Headshot image dataset from istockphoto. https://huggingface.co/datasets/BKM1804/headshot_istockphoto, 2025. Accessed: 2025-11-05, 6 000 images. 3, 10
- [5] BKM1804. headshot_pexels_v1: High-resolution headshot dataset from pexels. https://huggingface.co/datasets/BKM1804/headshot_pexels_v1, 2025. Accessed: 2025-11-05, includes 3 000 images. 3, 10
- [6] Tim Brooks, Aleksander Holynski, and Alexei A. Efros. Instructpix2pix: Learning to follow image editing instructions, 2023. 1
- [7] Siyu Cao, Hangting Chen, Peng Chen, Yiji Cheng, Yutao Cui, Xincheng Deng, Ying Dong, Kipper Gong, Tianpeng Gu, Xiusen Gu, Tiankai Hang, Duojuan Huang, Jie Jiang, Zhengkai Jiang, Weijie Kong, Changlin Li, Donghao Li, Junzhe Li, Xin Li, Yang Li, Zhenxi Li, Zhimin Li, Jiaxin Lin, Linus, Lucas Liu, Shu Liu, Songtao Liu, Yu Liu, Yuhong Liu, Yanxin Long, Fanbin Lu, Qinglin Lu, Yuyang Peng, Yuanbo Peng, Xiangwei Shen, Yixuan Shi, Jiale Tao, Yangyu Tao, Qi Tian, Pengfei Wan, Chunyu Wang, Kai Wang, Lei Wang, Linqing Wang, Lucas Wang, Qixun Wang, Weiyan Wang, Hao Wen, Bing Wu, Jianbing Wu, Yue Wu, Senhao Xie, Fang Yang, Miles Yang, Xiaofeng Yang, Xuan Yang, Zhan-tao Yang, Jingmiao Yu, Zheng Yuan, Chao Zhang, Jian-Wei Zhang, Peizhen Zhang, Shi-Xue Zhang, Tao Zhang, Weigang Zhang, Yepeng Zhang, Yingfang Zhang, Zihao Zhang, Zijian Zhang, Penghao Zhao, Zhiyuan Zhao, Xuefei Zhe, Jianchen Zhu, and Zhao Zhong. Hunyuanimage 3.0 technical report, 2025. 1
- [8] Soravit Changpinyo, Piyush Sharma, Nan Ding, and Radu Soricut. Conceptual 12m: Pushing web-scale image-text pre-training to recognize long-tail visual concepts, 2021. 6, 10
- [9] Bowen Chen, Mengyi Zhao, Haomiao Sun, Li Chen, Xu Wang, Kang Du, and Xinglong Wu. Xverse: Consistent multi-subject control of identity and semantic attributes via dit modulation, 2025. 1, 3
- [10] Hong Chen, Yipeng Zhang, Simin Wu, Xin Wang, Xuguang Duan, Yuwei Zhou, and Wenwu Zhu. Disenbooth: Identity-preserving disentangled tuning for subject-driven text-to-image generation, 2024. 1
- [11] Junsong Chen, Jincheng Yu, Chongjian Ge, Lewei Yao, Enze Xie, Yue Wu, Zhongdao Wang, James Kwok, Ping Luo, Huchuan Lu, and Zhenguo Li. Pixart- α : Fast training of diffusion transformer for photorealistic text-to-image synthesis, 2023. 1
- [12] Jiuhai Chen, Zhiyang Xu, Xichen Pan, Yushi Hu, Can Qin, Tom Goldstein, Lifu Huang, Tianyi Zhou, Saining Xie, Silvio Savarese, Le Xue, Caiming Xiong, and Ran Xu. Blip3-o: A family of fully open unified multimodal models-architecture, training and dataset, 2025. 2, 8, 11, 13
- [13] Jiuhai Chen, Le Xue, Zhiyang Xu, Xichen Pan, Shusheng Yang, Can Qin, An Yan, Honglu Zhou, Zeyuan Chen, Lifu Huang, Tianyi Zhou, Junnan Li, Silvio Savarese, Caiming Xiong, and Ran Xu. Blip3o-next: Next frontier of native image generation, 2025. 8
- [14] Yuzhuo Chen, Zehua Ma, Jianhua Wang, Kai Kang, Shunyu Yao, and Weiming Zhang. Lamic: Layout-aware multi-image composition via scalability of multimodal diffusion transformer, 2025. 1, 3
- [15] Seunghwan Choi, Sunghyun Park, Minsoo Lee, and Jaegul Choo. Viton-hd: High-resolution virtual try-on via misalignment-aware normalization, 2021. 3, 10
- [16] Siying Cui, Jia Guo, Xiang An, Jiankang Deng, Yongle Zhao, Xinyu Wei, and Ziyong Feng. Idadapter: Learning mixed features for tuning-free personalization of text-to-image models. In *Proceedings of the IEEE/CVF Conference on Computer Vision and Pattern Recognition (CVPR) Workshops*, pages 950–959, 2024. 1
- [17] Siying Cui, Jia Guo, Xiang An, Jiankang Deng, Yongle Zhao, Xinyu Wei, and Ziyong Feng. Idadapter: Learning mixed features for tuning-free personalization of text-to-image models, 2024. 1
- [18] Google DeepMind. Introducing gemini 1.5 flash: Fast, efficient, and multimodal. <https://developers.googleblog.com/en/introducing-gemini-2-5-flash-image/>, 2024. Accessed: 2025-10-18. 1, 2, 4, 5, 7, 10, 12, 13, 14
- [19] Chaorui Deng, Deyao Zhu, Kunchang Li, Chenhui Gou, Feng Li, Zeyu Wang, Shu Zhong, Weihao Yu, Xiaonan Nie, Ziang Song, Guang Shi, and Haoqi Fan. Emerging properties in unified multimodal pretraining. *arXiv preprint arXiv:2505.14683*, 2025. 2, 8, 11, 13
- [20] Chaorui Deng, Deyao Zhu, Kunchang Li, Chenhui Gou, Feng Li, Zeyu Wang, Shu Zhong, Weihao Yu, Xiaonan Nie, Ziang Song, Guang Shi, and Haoqi Fan. Emerging properties in unified multimodal pretraining, 2025. 1
- [21] Jiankang Deng, Jia Guo, Jing Yang, Niannan Xue, Irene Kotsoia, and Stefanos Zafeiriou. Arcface: Additive angular margin loss for deep face recognition. *IEEE Transactions on Pattern Analysis and Machine Intelligence*, 44(10):5962–5979, 2022. 4, 6, 7, 12
- [22] Patrick Esser, Sumith Kulal, Andreas Blattmann, Rahim Entezari, Jonas Müller, Harry Saini, Yam Levi, Dominik Lorenz, Axel Sauer, Frederic Boesel, Dustin Podell, Tim

- Dockhorn, Zion English, Kyle Lacey, Alex Goodwin, Yannik Marek, and Robin Rombach. Scaling rectified flow transformers for high-resolution image synthesis, 2024. 1
- [23] Martin Ester, Hans-Peter Kriegel, Jörg Sander, and Xiaowei Xu. A density-based algorithm for discovering clusters in large spatial databases with noise. In *Knowledge Discovery and Data Mining*, 1996. 3
- [24] Yu Gao, Lixue Gong, Qiushan Guo, Xiaoxia Hou, Zhichao Lai, Fanshi Li, Liang Li, Xiaochen Lian, Chao Liao, Liyang Liu, Wei Liu, Yichun Shi, Shiqi Sun, Yu Tian, Zhi Tian, Peng Wang, Rui Wang, Xuanda Wang, Xun Wang, Ye Wang, Guofeng Wu, Jie Wu, Xin Xia, Xuefeng Xiao, Zhonghua Zhai, Xinyu Zhang, Qi Zhang, Yuwei Zhang, Shijia Zhao, Jianchao Yang, and Weilin Huang. Seedream 3.0 technical report, 2025. 1
- [25] Lixue Gong, Xiaoxia Hou, Fanshi Li, Liang Li, Xiaochen Lian, Fei Liu, Liyang Liu, Wei Liu, Wei Lu, Yichun Shi, Shiqi Sun, Yu Tian, Zhi Tian, Peng Wang, Xun Wang, Ye Wang, Guofeng Wu, Jie Wu, Xin Xia, Xuefeng Xiao, Linjie Yang, Zhonghua Zhai, Xinyu Zhang, Qi Zhang, Yuwei Zhang, Shijia Zhao, Jianchao Yang, and Weilin Huang. Seedream 2.0: A native chinese-english bilingual image generation foundation model, 2025. 1
- [26] Zinan Guo, Yanze Wu, Zhuowei Chen, Lang Chen, Peng Zhang, and Qian He. Pulid: Pure and lightning id customization via contrastive alignment, 2024. 1, 3
- [27] Ziyu Guo, Xinyan Chen, Renrui Zhang, Ruichuan An, Yu Qi, Dongzhi Jiang, Xiangtai Li, Manyuan Zhang, Hongsheng Li, and Pheng-Ann Heng. Are video models ready as zero-shot reasoners? an empirical study with the mme-cof benchmark. *arXiv preprint arXiv:2510.26802*, 2025. 14
- [28] Ziyu Guo, Renrui Zhang, Hongyu Li, Manyuan Zhang, Xinyan Chen, Sifan Wang, Yan Feng, Peng Pei, and Pheng-Ann Heng. Thinking-while-generating: Interleaving textual reasoning throughout visual generation. *arXiv preprint arXiv:2511.16671*, 2025. 1
- [29] Ziyu Guo, Renrui Zhang, Chengzhuo Tong, Zhizheng Zhao, Rui Huang, Haoquan Zhang, Manyuan Zhang, Jiaming Liu, Shanghang Zhang, Peng Gao, et al. Can we generate images with cot? let's verify and reinforce image generation step by step. *arXiv preprint arXiv:2501.13926*, 2025. 1
- [30] Xiwei Hu, Rui Wang, Yixiao Fang, Bin Fu, Pei Cheng, and Gang Yu. Ella: Equip diffusion models with llm for enhanced semantic alignment, 2024. 14
- [31] Qihan Huang, Siming Fu, Jinlong Liu, Hao Jiang, Yipeng Yu, and Jie Song. Resolving multi-condition confusion for finetuning-free personalized image generation, 2024. 1, 3
- [32] Dongzhi Jiang, Ziyu Guo, Renrui Zhang, Zhuofan Zong, Hao Li, Le Zhuo, Shilin Yan, Pheng-Ann Heng, and Hongsheng Li. T2i-r1: Reinforcing image generation with collaborative semantic-level and token-level cot. *arXiv preprint arXiv:2505.00703*, 2025. 1
- [33] Alexander Kirillov, Eric Mintun, Nikhila Ravi, Hanzi Mao, Chloe Rolland, Laura Gustafson, Tete Xiao, Spencer Whitehead, Alexander C. Berg, Wan-Yen Lo, Piotr Dollár, and Ross Girshick. Segment anything, 2023. 1, 2, 3
- [34] Max Ku, Dongfu Jiang, Cong Wei, Xiang Yue, and Wenhua Chen. Viescore: Towards explainable metrics for conditional image synthesis evaluation, 2024. 7
- [35] Harold W. Kuhn. The hungarian method for the assignment problem. *Naval Research Logistics (NRL)*, 52, 1955. 6
- [36] Black Forest Labs. Flux.1 – official inference repository for flux models. <https://github.com/black-forest-labs/flux>, 2024. Accessed: 2025-10-18. 1
- [37] Black Forest Labs, Stephen Batifol, Andreas Blattmann, Frederic Boesel, Saksham Consul, Cyril Diagne, Tim Dockhorn, Jack English, Zion English, Patrick Esser, Sumith Kulal, Kyle Lacey, Yam Levi, Cheng Li, Dominik Lorenz, Jonas Müller, Dustin Podell, Robin Rombach, Harry Saini, Axel Sauer, and Luke Smith. Flux.1 kontext: Flow matching for in-context image generation and editing in latent space, 2025. 1, 6
- [38] Zhen Li, Mingdeng Cao, Xintao Wang, Zhongang Qi, Ming-Ming Cheng, and Ying Shan. Photomaker: Customizing realistic human photos via stacked id embedding, 2023. 1
- [39] Zhimin Li, Jianwei Zhang, Qin Lin, Jiangfeng Xiong, Yanxin Long, Xincheng Deng, Yingfang Zhang, Xingchao Liu, Minbin Huang, Zedong Xiao, Dayou Chen, Jiajun He, Jiahao Li, Wenyue Li, Chen Zhang, Rongwei Quan, Jianxiang Lu, Jiabin Huang, Xiaoyan Yuan, Xiaoxiao Zheng, Yixuan Li, Jihong Zhang, Chao Zhang, Meng Chen, Jie Liu, Zheng Fang, Weiyan Wang, Jinbao Xue, Yangyu Tao, Jianchen Zhu, Kai Liu, Sihuan Lin, Yifu Sun, Yun Li, Dongdong Wang, Mingtao Chen, Zhichao Hu, Xiao Xiao, Yan Chen, Yuhong Liu, Wei Liu, Di Wang, Yong Yang, Jie Jiang, and Qinglin Lu. Hunyuan-dit: A powerful multi-resolution diffusion transformer with fine-grained chinese understanding, 2024. 1
- [40] Weifeng Lin, Ziheng Wu, Jiayu Chen, Jun Huang, and Lianwen Jin. Scale-aware modulation meet transformer. In *Proceedings of the IEEE/CVF International Conference on Computer Vision (ICCV)*, pages 6015–6026, 2023. 12
- [41] Weifeng Lin, Xinyu Wei, Ruichuan An, Peng Gao, Bocheng Zou, Yulin Luo, Siyuan Huang, Shanghang Zhang, and Hongsheng Li. Draw-and-understand: Leveraging visual prompts to enable mllms to comprehend what you want. *arXiv preprint arXiv:2403.20271*, 2024. 12
- [42] Weifeng Lin, Xinyu Wei, Renrui Zhang, Le Zhuo, Shitian Zhao, Siyuan Huang, Huan Teng, Junlin Xie, Yu Qiao, Peng Gao, et al. Pixwizard: Versatile image-to-image visual assistant with open-language instructions. *arXiv preprint arXiv:2409.15278*, 2024. 1
- [43] Weifeng Lin, Xinyu Wei, Ruichuan An, Tianhe Ren, Tingwei Chen, Renrui Zhang, Ziyu Guo, Wentao Zhang, Lei Zhang, and Hongsheng Li. Perceive anything: Recognize, explain, caption, and segment anything in images and videos. *arXiv preprint arXiv:2506.05302*, 2025. 12
- [44] Shilong Liu, Zhaoyang Zeng, Tianhe Ren, Feng Li, Hao Zhang, Jie Yang, Qing Jiang, Chunyuan Li, Jianwei Yang, Hang Su, Jun Zhu, and Lei Zhang. Grounding dino: Marrying dino with grounded pre-training for open-set object detection, 2024. 1, 2, 3
- [45] Shiyu Liu, Yucheng Han, Peng Xing, Fukun Yin, Rui Wang, Wei Cheng, Jiaqi Liao, Yingming Wang, Honghao Fu, Chunrui Han, Guopeng Li, Yuang Peng, Quan Sun, Jingwei Wu,

- Yan Cai, Zheng Ge, Ranchen Ming, Lei Xia, Xianfang Zeng, Yibo Zhu, Binxing Jiao, Xiangyu Zhang, Gang Yu, and Daxin Jiang. Step1x-edit: A practical framework for general image editing, 2025. 1
- [46] Yulin Luo, Ruichuan An, Bocheng Zou, Yiming Tang, Jiaming Liu, and Shanghang Zhang. Llm as dataset analyst: Subpopulation structure discovery with large language model. In *European Conference on Computer Vision*, pages 235–252. Springer, 2024. 12
- [47] Jian Ma, Junhao Liang, Chen Chen, and Haonan Lu. Subject-diffusion: open domain personalized text-to-image generation without test-time fine-tuning, 2024. 1, 3
- [48] Chong Mou, Xintao Wang, Liangbin Xie, Yanze Wu, Jian Zhang, Zhongang Qi, Ying Shan, and Xiaohu Qie. T2i-adapter: Learning adapters to dig out more controllable ability for text-to-image diffusion models, 2023. 1
- [49] Chong Mou, Yanze Wu, Wenxu Wu, Zinan Guo, Pengze Zhang, Yufeng Cheng, Yiming Luo, Fei Ding, Shiwen Zhang, Xinghui Li, Mengtian Li, Mingcong Liu, Yi Zhang, Shaojin Wu, Songtao Zhao, Jian Zhang, Qian He, and Xinglong Wu. Dreamo: A unified framework for image customization, 2025. 1, 3
- [50] OpenAI. Dall-e 3. <https://openai.com/index/dall-e-3/>, 2023. Accessed: 2025-10-14. 1
- [51] OpenAI. Gpt-4o image generation. <https://openai.com/index/introducing-4o-image-generation/>, 2025. Accessed: 2025-10-18. 1, 2, 10, 12, 13, 14
- [52] Maxime Oquab, Timothée Darcet, Théo Moutakanni, Huy Vo, Marc Szafraniec, Vasil Khalidov, Pierre Fernandez, Daniel Haziza, Francisco Massa, Alaaeldin El-Nouby, Mahmoud Assran, Nicolas Ballas, Wojciech Galuba, Russell Howes, Po-Yao Huang, Shang-Wen Li, Ishan Misra, Michael Rabbat, Vasu Sharma, Gabriel Synnaeve, Hu Xu, Hervé Jegou, Julien Mairal, Patrick Labatut, Armand Joulin, and Piotr Bojanowski. Dinov2: Learning robust visual features without supervision, 2024. 13
- [53] Maitreya Patel, Tejas Gokhale, Chitta Baral, and Yezhou Yang. Conceptbed: Evaluating concept learning abilities of text-to-image diffusion models, 2024. 1
- [54] Maitreya Patel, Sangmin Jung, Chitta Baral, and Yezhou Yang. λ -eclipse: Multi-concept personalized text-to-image diffusion models by leveraging clip latent space, 2024. 1, 3
- [55] Dustin Podell, Zion English, Kyle Lacey, Andreas Blattmann, Tim Dockhorn, Jonas Müller, Joe Penna, and Robin Rombach. Sdxl: Improving latent diffusion models for high-resolution image synthesis, 2023. 1
- [56] Can Qin, Shu Zhang, Ning Yu, Yihao Feng, Xinyi Yang, Yingbo Zhou, Huan Wang, Juan Carlos Niebles, Caiming Xiong, Silvio Savarese, Stefano Ermon, Yun Fu, and Ran Xu. Unicontrol: A unified diffusion model for controllable visual generation in the wild, 2023. 1
- [57] QwenLM. Qwen-image-edit-2509. <https://huggingface.co/Qwen/Qwen-Image-Edit-2509>, 2025. Accessed: 2025-11-12. 3, 8, 15
- [58] Nikhila Ravi, Valentin Gabeur, Yuan-Ting Hu, Ronghang Hu, Chaitanya Ryali, Tengyu Ma, Haitham Khedr, Roman Rädle, Chloe Rolland, Laura Gustafson, Eric Mintun, Junting Pan, Kalyan Vasudev Alwala, Nicolas Carion, Chao-Yuan Wu, Ross Girshick, Piotr Dollár, and Christoph Feichtenhofer. Sam 2: Segment anything in images and videos, 2024. 15
- [59] Robin Rombach, Andreas Blattmann, Dominik Lorenz, Patrick Esser, and Björn Ommer. High-resolution image synthesis with latent diffusion models, 2022. 1
- [60] Nataniel Ruiz, Yuanzhen Li, Varun Jampani, Yael Pritch, Michael Rubinstein, and Kfir Aberman. Dreambooth: Fine tuning text-to-image diffusion models for subject-driven generation, 2023. 1
- [61] Nataniel Ruiz, Yuanzhen Li, Varun Jampani, Wei Wei, Tingbo Hou, Yael Pritch, Neal Wadhwa, Michael Rubinstein, and Kfir Aberman. Hyperdreambooth: Hypernetworks for fast personalization of text-to-image models, 2024. 1
- [62] Team Seedream, Yunpeng Chen, Yu Gao, Lixue Gong, Meng Guo, Qiushan Guo, Zhiyao Guo, Xiaoxia Hou, Weilin Huang, Yixuan Huang, Xiaowen Jian, Huafeng Kuang, Zhichao Lai, Fanshi Li, Liang Li, Xiaochen Lian, Chao Liao, Liyang Liu, Wei Liu, Yanzuo Lu, Zhengxiong Luo, Tongtong Ou, Guang Shi, Yichun Shi, Shiqi Sun, Yu Tian, Zhi Tian, Peng Wang, Rui Wang, Xun Wang, Ye Wang, Guofeng Wu, Jie Wu, Wenxu Wu, Yonghui Wu, Xin Xia, Xuefeng Xiao, Shuang Xu, Xin Yan, Ceyuan Yang, Jianchao Yang, Zhonghua Zhai, Chenlin Zhang, Heng Zhang, Qi Zhang, Xinyu Zhang, Yuwei Zhang, Shijia Zhao, Wenliang Zhao, and Wenjia Zhu. Seedream 4.0: Toward next-generation multimodal image generation, 2025. 1
- [63] Jerry Sima, Eric Cheng, William Fedus, Miles Brundage, Mark Chen, Iason Gabriel, Sandhini Agarwal, Lilian Weng, et al. Addendum to gpt-4o system card: Native image capabilities. <https://www.semanticscholar.org/paper/0c9b799e0dde7dcbe42f8dc61b242a0106739eba>, 2024. Accessed: 2025-10-18. 1
- [64] Oriane Siméoni, Huy V. Vo, Maximilian Seitzer, Federico Baldassarre, Maxime Oquab, Cijo Jose, Vasil Khalidov, Marc Szafraniec, Seungeun Yi, Michaël Ramamonjisoa, Francisco Massa, Daniel Haziza, Luca Wehrstedt, Jianyuan Wang, Timothée Darcet, Théo Moutakanni, Leonel Sentana, Claire Roberts, Andrea Vedaldi, Jamie Tolan, John Brandt, Camille Couprie, Julien Mairal, Hervé Jégou, Patrick Labatut, and Piotr Bojanowski. Dinov3, 2025. 3
- [65] Wensong Song, Hong Jiang, Zongxing Yang, Ruijie Quan, and Yi Yang. Insert anything: Image insertion via in-context editing in dit, 2025. 1
- [66] Zhenxiong Tan, Songhua Liu, Xingyi Yang, Qiaochu Xue, and Xinchao Wang. Ominicontrol: Minimal and universal control for diffusion transformer, 2025. 3, 10
- [67] OpenAI Team. Gpt-4o system card, 2024. 4, 6, 7, 13
- [68] Darian Tomašević, Fadi Boutros, Chenhao Lin, Naser Damer, Vitomir Štruc, and Peter Peer. Id-booth: Identity-consistent face generation with diffusion models. In *2025 IEEE 19th International Conference on Automatic Face and Gesture Recognition (FG)*, page 1–10. IEEE, 2025. 1
- [69] Chengzhuo Tong, Ziyu Guo, Renrui Zhang, Wenyu Shan, Xinyu Wei, Zhenghao Xing, Hongsheng Li, and Pheng-Ann

- Heng. Delving into rl for image generation with cot: A study on dpo vs. grpo. *arXiv preprint arXiv:2505.17017*, 2025. 12
- [70] Chengzhuo Tong, Ziyu Guo, Renrui Zhang, Wenyu Shan, Xinyu Wei, Zhenghao Xing, Hongsheng Li, and Pheng-Ann Heng. Delving into rl for image generation with cot: A study on dpo vs. grpo, 2025. 1
- [71] Michael Tschanen, Alexey Gritsenko, Xiao Wang, Muhammad Ferjad Naeem, Ibrahim Alabdulmohsin, Nikhil Parthasarathy, Talfan Evans, Lucas Beyer, Ye Xia, Basil Mustafa, Olivier Hénaff, Jeremiah Harmsen, Andreas Steiner, and Xiaohua Zhai. Siglip 2: Multilingual vision-language encoders with improved semantic understanding, localization, and dense features, 2025. 3
- [72] Petru-Daniel Tudosiu, Yongxin Yang, Shifeng Zhang, Fei Chen, Steven McDonagh, Gerasimos Lampouras, Ignacio Iacobacci, and Sarah Parisot. Mulan: A multi layer annotated dataset for controllable text-to-image generation, 2024. 3, 10
- [73] Guanqun Wang, Jiaming Liu, Chenxuan Li, Yuan Zhang, Junpeng Ma, Xinyu Wei, Kevin Zhang, Maurice Chong, Renrui Zhang, Yijiang Liu, and Shanghang Zhang. Cloud-device collaborative learning for multimodal large language models. In *Proceedings of the IEEE/CVF Conference on Computer Vision and Pattern Recognition (CVPR)*, pages 12646–12655, 2024. 12
- [74] Guanqun Wang, Xinyu Wei, Jiaming Liu, Ray Zhang, Yichi Zhang, Kevin Zhang, Maurice Chong, and Shanghang Zhang. Mr-mllm: Mutual reinforcement of multimodal comprehension and vision perception. *arXiv preprint arXiv:2406.15768*, 2024. 12
- [75] Peiyu Wang, Yi Peng, Yimeng Gan, Liang Hu, Tianyidan Xie, Xiaokun Wang, Yichen Wei, Chuanxin Tang, Bo Zhu, Changshi Li, Hongyang Wei, Eric Li, Xuchen Song, Yang Liu, and Yahui Zhou. Skywork unipic: Unified autoregressive modeling for visual understanding and generation, 2025. 1
- [76] Peng Wang, Yichun Shi, Xiaochen Lian, Zhonghua Zhai, Xin Xia, Xuefeng Xiao, Weilin Huang, and Jianchao Yang. Seedit 3.0: Fast and high-quality generative image editing, 2025. 1
- [77] Qixun Wang, Xu Bai, Haofan Wang, Zekui Qin, Anthony Chen, Huaxia Li, Xu Tang, and Yao Hu. Instantid: Zero-shot identity-preserving generation in seconds, 2024. 1
- [78] Xierui Wang, Siming Fu, Qihan Huang, Wanggui He, and Hao Jiang. Ms-diffusion: Multi-subject zero-shot image personalization with layout guidance, 2025. 1, 3
- [79] Zeqing Wang, Xinyu Wei, Bairui Li, Zhen Guo, Jinrui Zhang, Hongyang Wei, Keze Wang, and Lei Zhang. Video-verse: How far is your t2v generator from a world model? *arXiv preprint arXiv:2510.08398*, 2025. 14
- [80] Hongyang Wei, Shuaizheng Liu, Chun Yuan, and Lei Zhang. Perceive, understand and restore: Real-world image super-resolution with autoregressive multimodal generative models, 2025. 1
- [81] Hongyang Wei, Baixin Xu, Hongbo Liu, Cyrus Wu, Jie Liu, Yi Peng, Peiyu Wang, Zexiang Liu, Jingwen He, Yidan Xietian, Chuanxin Tang, Zidong Wang, Yichen Wei, Liang Hu, Boyi Jiang, William Li, Ying He, Yang Liu, Xuchen Song, Eric Li, and Yahui Zhou. Skywork unipic 2.0: Building context model with online rl for unified multimodal model, 2025. 1
- [82] Xinyu Wei, Jinrui Zhang, Zeqing Wang, Hongyang Wei, Zhen Guo, and Lei Zhang. Tiif-bench: How does your t2i model follow your instructions? *arXiv preprint arXiv:2506.02161*, 2025. 14
- [83] Chenfei Wu, Jiahao Li, Jingren Zhou, Junyang Lin, Kaiyuan Gao, Kun Yan, Sheng ming Yin, Shuai Bai, Xiao Xu, Yilei Chen, Yuxiang Chen, Zecheng Tang, Zekai Zhang, Zhengyi Wang, An Yang, Bowen Yu, Chen Cheng, Dayiheng Liu, Deqing Li, Hang Zhang, Hao Meng, Hu Wei, Jingyuan Ni, Kai Chen, Kuan Cao, Liang Peng, Lin Qu, Minggang Wu, Peng Wang, Shuting Yu, Tingkun Wen, Wensen Feng, Xiaoxiao Xu, Yi Wang, Yichang Zhang, Yongqiang Zhu, Yujia Wu, Yuxuan Cai, and Zenan Liu. Qwen-image technical report, 2025. 1, 2, 8, 11, 13
- [84] Chenyuan Wu, Pengfei Zheng, Ruirao Yan, Shitao Xiao, Xin Luo, Yueze Wang, Wanli Li, Xiyan Jiang, Yexin Liu, Junjie Zhou, Ze Liu, Ziyi Xia, Chaofan Li, Haoge Deng, Jiahao Wang, Kun Luo, Bo Zhang, Defu Lian, Xinlong Wang, Zhongyuan Wang, Tiejun Huang, and Zheng Liu. Omnigen2: Exploration to advanced multimodal generation, 2025. 1, 2, 3, 7, 8, 11, 13
- [85] Shaojin Wu, Mengqi Huang, Wenxu Wu, Yufeng Cheng, Fei Ding, and Qian He. Less-to-more generalization: Unlocking more controllability by in-context generation, 2025. 1, 3
- [86] Bin Xia, Bohao Peng, Yuechen Zhang, Junjie Huang, Jiyang Liu, Jingyao Li, Haoru Tan, Sitong Wu, Chengyao Wang, Yitong Wang, Xinglong Wu, Bei Yu, and Jiayia Jia. Dreamomni2: Multimodal instruction-based editing and generation, 2025. 2, 3
- [87] Jianxiong Xiao, James Hays, Krista A. Ehinger, Aude Oliva, and Antonio Torralba. Sun database: Large-scale scene recognition from abbey to zoo. In *2010 IEEE Computer Society Conference on Computer Vision and Pattern Recognition*, pages 3485–3492, 2010. 3, 10
- [88] Shitao Xiao, Yueze Wang, Junjie Zhou, Huaying Yuan, Xingrun Xing, Ruirao Yan, Chaofan Li, Shuting Wang, Tiejun Huang, and Zheng Liu. Omnigen: Unified image generation, 2024. 3, 10
- [89] Yi Xin, Qi Qin, Siqi Luo, Kaiwen Zhu, Juncheng Yan, Yan Tai, Jiayi Lei, Yuewen Cao, Keqi Wang, Yibin Wang, Jinbin Bai, Qian Yu, Dengyang Jiang, Yuandong Pu, Haoxing Chen, Le Zhuo, Junjun He, Gen Luo, Tianbin Li, Ming Hu, Jin Ye, Shenglong Ye, Bo Zhang, Chang Xu, Wenhui Wang, Hongsheng Li, Guangtao Zhai, Tianfan Xue, Bin Fu, Xiaohong Liu, Yu Qiao, and Yihao Liu. Lumina-dimoo: An omni diffusion large language model for multi-modal generation and understanding, 2025. 2, 8, 11, 13
- [90] Hengyuan Xu, Wei Cheng, Peng Xing, Yixiao Fang, Shuhan Wu, Rui Wang, Xianfang Zeng, Daxin Jiang, Gang Yu, Xingjun Ma, and Yu-Gang Jiang. Withanyone: Towards controllable and id consistent image generation, 2025. 12
- [91] Xingqian Xu, Zhangyang Wang, Eric Zhang, Kai Wang, and Humphrey Shi. Versatile diffusion: Text, images and variations all in one diffusion model, 2024. 1, 3

- [92] Hu Ye, Jun Zhang, Sibao Liu, Xiao Han, and Wei Yang. Ip-adapter: Text compatible image prompt adapter for text-to-image diffusion models, 2023. [1](#)
- [93] Junyan Ye, Zihao Wang, Dongzhi Jiang, Leqi Zhu, Zhenghao Hu, Zilong Huang, Jun He, Zhiyuan Yan, Jinghua Yu, Hongsheng Li, Conghui He, and Weijia Li. Echo-4o: Harnessing the power of gpt-4o synthetic images for improved image generation. <https://arxiv.org/abs/2508.09987>, 2025. [1](#), [3](#), [6](#), [10](#)
- [94] Kai Zhang, Lingbo Mo, Wenhui Chen, Huan Sun, and Yu Su. Magicbrush: A manually annotated dataset for instruction-guided image editing, 2024. [1](#)
- [95] Lvmin Zhang, Anyi Rao, and Maneesh Agrawala. Adding conditional control to text-to-image diffusion models, 2023. [1](#)
- [96] Renrui Zhang, Xinyu Wei, Dongzhi Jiang, Ziyu Guo, Shicheng Li, Yichi Zhang, Chengzhuo Tong, Jiaming Liu, Aojun Zhou, Bin Wei, et al. Mavis: Mathematical visual instruction tuning with an automatic data engine. *arXiv preprint arXiv:2407.08739*, 2024. [12](#)
- [97] Zechuan Zhang, Ji Xie, Yu Lu, Zongxin Yang, and Yi Yang. In-context edit: Enabling instructional image editing with in-context generation in large scale diffusion transformer, 2025. [1](#)